Atmos. Chem. Phys., 13, 4749–4781, 2013
www.atmos-chem-phys.net/13/4749/2013/
doi:10.5194/acp-13-4749-2013

Atmospheric Chemistry and Physics Open Access

Systematic investigation of bromine monoxide in volcanic plumes from space by using the GOME-2 instrument

C. Hörmann[1,2], H. Sihler[1,2], N. Bobrowski[2], S. Beirle[1], M. Penning de Vries[1], U. Platt[2], and T. Wagner[1]

[1]Max Planck Institute for Chemistry, Mainz, Germany
[2]Institute for Environmental Physics, University of Heidelberg, Heidelberg, Germany

Correspondence to: C. Hörmann (c.hoermann@mpic.de)

Received: 12 September 2012 – Published in Atmos. Chem. Phys. Discuss.: 15 November 2012
Revised: 15 March 2013 – Accepted: 28 March 2013 – Published: 8 May 2013

Abstract. During recent years, volcanic emissions turned out to be a natural source of bromine compounds in the atmosphere. While the initial formation process of bromine monoxide (BrO) has been successfully studied in local ground-based measurements at quiescent degassing volcanoes worldwide, literature on the chemical evolution of BrO on large spatial and temporal scales is sparse. The first space-based observation of a volcanic BrO plume following the Kasatochi eruption in 2008 demonstrated the capability of satellite instruments to monitor such events on a global scale.

In this study, we systematically examined GOME-2 observations from January 2007 until June 2011 for significantly enhanced BrO slant column densities (SCDs) in the vicinity of volcanic plumes. In total, 772 plumes from at least 37 volcanoes have been found by using sulphur dioxide (SO_2) as a tracer for a volcanic plume. All captured SO_2 plumes were subsequently analysed for a simultaneous enhancement of BrO and the data were checked for a possible spatial correlation between the two species. Additionally, the mean BrO/SO_2 ratios for all volcanic plumes have been calculated by the application of a bivariate linear fit.

A total number of 64 volcanic plumes from at least 11 different volcanoes showed clear evidence for BrO of volcanic origin, revealing large differences in the BrO/SO_2 ratios (ranging from some 10^{-5} to several 10^{-4}) and the spatial distribution of both species. A close correlation between SO_2 and BrO occurred only for some of the observed eruptions or just in certain parts of the examined plumes. For other cases, only a rough spatial relationship was found. We discuss possible explanations for the occurrence of the different spatial SO_2 and BrO distributions in aged volcanic plumes.

1 Introduction

BrO is an important catalyst in the depletion of ozone (O_3) in the stratosphere and troposphere, especially during springtime in polar regions (see Barrie et al., 1988; Solomon, 1999; Rowland, 2006; Simpson et al., 2007, and references therein). In addition to sources like the surfaces of salt lakes, polar sea ice or sea-salt aerosol in the mid-latitude marine boundary layer (von Glasow and Crutzen, 2003), volcanic emissions turned out to be a further natural source of bromine compounds and the subsequent formation of BrO (Bobrowski et al., 2003). The injection of BrO that has formed in volcanic plumes is, therefore, very likely to have a significant impact on atmospheric chemistry (von Glasow, 2010).

BrO in a volcanic plume was detected for the first time by Bobrowski et al. (2003), using ground-based Multi-Axis Differential Optical Absorption Spectroscopy (MAX-DOAS) measurements at the Soufrière Hills volcano on Montserrat. The BrO slant column densities (SCDs) were found to be closely correlated to the measured SO_2 SCDs, resulting in an average BrO/SO_2 molar ratio of $\sim 8.2 \times 10^{-4}$ (equal to a Br/S mass ratio of $\sim 2 \times 10^{-3}$). Based on this ratio, the authors estimated a global emission of 30 000 t Br yr^{-1} using the estimation of the global volcanic SO_2-source-strength of about 14 ± 6 Tg SO_2 yr^{-1} by Graf et al. (1997). Since then, similar ground-based observations were made at several volcanoes worldwide (e.g. Galle et al., 2005; Oppenheimer et al., 2006; Bobrowski and Platt, 2007; Boichu et al., 2011, and references therein). All these measurements revealed an almost linear correlation between the two species and typical BrO/SO_2 molar ratios ranging from 1×10^{-5} to 8.2×10^{-4}.

In addition to the ground-based measurements, BrO has also been detected by airborne observations of volcanic plumes during the recent years (e.g. Bani et al., 2009; Heue et al., 2011; Kelly et al., 2012).

First considerations about the origin of BrO in volcanic plumes in Bobrowski et al. (2003) and Gerlach (2004) suggested that BrO is probably not directly emitted by volcanoes, but formed as a secondary product from near-vent, high-temperature oxidation of magmatic gases and heterogeneous chemistry involving sulphate aerosols inside the plume. Motivated by that suggestion, Oppenheimer et al. (2006) and Bobrowski et al. (2007) investigated the daytime plume of Mt. Etna (Sicily) at different distances, directly at the summit crater, but also further away at a plume age of a few minutes. As BrO was only observed in the downwind plume (not in the crater measurements), these findings widely agreed with the former predictions. The rapid production of BrO inside the downwind plume could, thus, be explained by directly emitted HBr, which is oxidised in an autocatalytic reaction cycle involving sulphate aerosols and solar radiation as well as the destruction of O_3. These procedures are associated with the mechanism known as the "bromine explosion", a reaction cycle that is closely related to the formation of BrO during polar spring and linked to tropospheric ozone depletion events (McConnell et al., 1992; Fan and Jacob, 1992; Platt and Lehrer, 1996; Wennberg, 1999; von Glasow and Crutzen, 2003; Simpson et al., 2007). As SO_2 is relatively inert compared to BrO, it can, for example, be used as a tracer to investigate ongoing BrO chemistry in ground-based measurements close to a volcano. The BrO/SO_2 ratio can be used as an indicator for the evolution of BrO in a plume, as aspects like plume dilution by ambient air, plume dispersion and varying emission strengths of the volcano are similar for both species and, thus, cancel out (Vogel, 2012).

Other studies by Bobrowski et al. (2007) and Louban et al. (2009) showed both enhanced BrO vertical column densities (VCDs) and BrO/SO_2 ratios toward the edges of the volcanic plume of Mt. Etna, in good agreement to model studies (Bobrowski et al., 2007; von Glasow, 2010), where the increase is caused by the entrainment of O_3-rich ambient air into the plume devoid of O_3. Additionally, a case study of day- and nighttime measurements at Masaya volcano (Nicaragua) by Kern et al. (2008), using Long Path Differential Optical Absorption Spectroscopy (LP-DOAS), showed no evidence for BrO during nighttime, while a BrO/SO_2 ratio of up to 6.4×10^{-5} was observed during daytime. This confirmed the suggestion that the reaction cycle is photolytically driven. Furthermore, the long-term dataset of BrO/SO_2 ratios from ground-based MAX-DOAS measurements at Mt. Etna during 2006–2009 has recently been investigated for its variability in relation to volcanic processes, and it was argued that the BrO/SO_2 ratio can serve as a parameter to indicate a volcano's state and, hence, as an precursor for the onset of eruptive activity (Bobrowski and Giuffrida, 2012).

Given the numerous spectroscopic BrO measurements in volcanic plumes and the general ability of satellite instruments to monitor BrO globally (e.g. Wagner and Platt, 1998; Richter et al., 2002; Theys et al., 2011), it appears like an obvious idea to investigate satellite data also for BrO during volcanic events. However, a first attempt to detect volcanic BrO from space, using data from the GOME and the SCIAMACHY (Scanning Imaging Absorption Spectrometer for Atmospheric Cartography) instruments, failed (Afe et al., 2004): No correlation between enhanced columns of SO_2 and the corresponding BrO columns was found in the plumes of selected eruptions at Mt. Etna, Popocatépetl (Mexico), the Soufrière Hills volcano and Nyamuragira (D.R. Congo). The authors investigated several reasons for the lack of enhanced BrO observations in this first study, including the reduced sensitivity of the satellite instruments and the actual absence of high BrO concentrations during these eruptions. As the size of a GOME ground-pixel is $40 \times 320\,km^2$, a volcanic BrO plume might be often invisible to satellite instruments, because the plume only covers a small fraction of the satellite ground-pixel. Thus, the signal from the plume is "diluted" by the radiation originating from the remaining (much larger) part of the pixel, which is not affected by the plume. Although the SCIAMACHY instrument provides a much higher spatial resolution ($30 \times 60\,km^2$) compared to GOME, it has the disadvantage of a rather sparse daily coverage of the troposphere due to the instrument's alternating limb/nadir observation sequence (Bovensmann et al., 1999). In addition, the signal-to-noise ratio in the UV range of SCIAMACHY is reduced due to a anomalously low grating efficiency (De Smedt et al., 2004).

The first detection of a volcanic BrO plume by a satellite instrument was eventually reported after the eruption of the Kasatochi volcano (Aleutian Islands) on 7 August 2008 by Theys et al. (2009a). The GOME-2 instrument (with an improved spatial resolution of $40 \times 80\,km^2$ compared to its precursor GOME) was able to track the plume for several days during its transport eastwards across the whole North American continent. Additionally, the authors reported that similar BrO SCDs were now also observed by SCIAMACHY and also a significant enhancement of BrO after the Mt. Etna eruption on 13 May 2008 was mentioned. Later, enhanced BrO VCDs were measured during the eruption of Eyjafjallajökull in 2010 simultaneously by both the GOME-2 instrument and the airborne CARIBIC (Civil Aircraft for the Regular Investigation of the atmosphere Based on an Instrument Container – for details about the project see Brenninkmeijer et al., 2007) DOAS instrument in the aged volcanic plume located north of Ireland (Heue et al., 2011). The measured SO_2 and BrO VCDs by CARIBIC and GOME-2 on 16 May 2010 were found to agree well, and BrO/SO_2 molar ratios of $1.2–1.3 \times 10^{-4}$ for the airborne measurements and a mean ratio of 1.3×10^{-4} for the GOME-2 measurements were determined in the same area. Furthermore, in the framework of a SO_2 comparison study between GOME-2 and the DLR

Falcon aircraft at Eyjafjallajökull, mean BrO/SO_2 ratios were calculated for some days of the satellite observations in May 2010 that varied from $1.1–2.1 \times 10^{-4}$ (Rix et al., 2012).

Motivated by these findings, we analysed the whole dataset of GOME-2 from the beginning of the regular measurements in January 2007 until the end of June 2011 in order to find further volcanic events in the satellite data where BrO might have been detected in the corresponding plumes. For that purpose, volcanic plumes were automatically extracted from the data by identifying clusters of significantly enhanced SO_2 SCDs. Since SO_2 is usually the third most abundant gaseous species emitted by volcanoes (e.g. Houghton et al., 2000; Textor et al., 2004) and is normally easy to detect in the UV due to its strong differential absorption features, it is well-suited as a proxy for the existence and extent of a volcanic plume. The area covered by each captured SO_2 plume was investigated for a simultaneous enhancement of BrO. Afterwards, the data were checked for the degree of spatial correlation between the two species and the BrO/SO_2 ratios were calculated.

The paper is structured as follows: After a short description of the GOME-2 satellite instrument and the DOAS retrieval for SO_2 and BrO in Sect. 2, the volcanic plume extraction algorithm, the background correction for non-volcanic BrO (respectively SO_2) and the approach for dealing with saturation effects in the SO_2 retrieval during major volcanic eruptions are introduced in Sect. 3. Section 4 presents the results, showing several examples for different BrO/SO_2 relationships from the identified volcanic plumes. Subsequently, in Sect. 5, all extracted volcanic plumes are systematically analysed and categorised according to their BrO/SO_2 relationship. A discussion of the results and conclusions are finally given in Sect. 6.

2 Instrument and data retrieval

The GOME-2 (Global Ozone Monitoring Experiment-2) is the first of three identical instruments that are part of the MetOp satellite series operated by the European Organisation for the Exploitation of Meteorological Satellites (EUMETSAT). MetOp-A was launched into a sun-synchronous polar orbit at 800 km altitude in October 2006 (Callies et al., 2000) (the second and third GOME-2 instrument will be carried by MetOp-B and MetOp-C in 2012 and 2018, respectively). The satellite crosses the equator at 09:30 local time. GOME-2 is a 4 channel UV/Vis grating spectrometer that observes the Earth's atmosphere in nadir viewing geometry. By scanning the earth surface with a swath-width of 1920 km (including viewing angles up to 50° off-nadir), global coverage is achieved within 1.5 days (EUMETSAT, 2005; Munro et al., 2006). GOME-2 measures both the radiance component of sunlight reflected by the Earth's atmosphere and the direct sunlight, covering the wavelength region of 240–790 nm at moderate spectral resolution of 0.2–0.4 nm. With a pixel size of $40 \times 80\,km^2$, GOME-2 observes 4 times smaller ground pixels than its predecessor GOME on ERS-2.

2.1 Standard DOAS retrieval for SO_2 and BrO

The satellite data were analysed using the Differential Optical Absorption Spectroscopy (DOAS) technique (Platt and Stutz, 2008). For our SO_2 standard retrieval (SO_2 SR), the wavelength range 312.1–324 nm was used. Apart from a cross section for SO_2 (Bogumil et al., 2003, 273 K), an O_3 cross section (Gür et al., 2005, 223 K), the individual Sun Mean Reference Spectrum (SMR) from GOME-2 for each day (containing no atmospheric absorptions), the Ring spectrum (calculated from the SMR – see Wagner et al., 2009) and the inverse SMR spectrum were included into the fitting process (the inverse SMR spectrum is a first-order correction for possible spectrographic stray light). In addition to the original O_3 absorption cross section, a second one (the original cross section scaled with λ^4) was included to consider the wavelength dependence of the O_3 airmass factor (AMF) caused by Rayleigh scattering (e.g. Van Roozendael et al., 2006a; Pukīte et al., 2010). By including this second O_3 reference spectrum, the fit residual can be reduced appreciably, especially for strong ozone absorption at large SZA. A 5th order polynomial was applied to account for the broad-band structures and a small wavelength shift was allowed for the measured spectra.

For the BrO retrieval, the wavelength range from 336–360 nm was used, which contains 4 adjacent absorption bands (Sihler et al., 2012). In addition to the BrO cross section from Wilmouth et al. (1999, 228 K), ozone cross sections at 223 and 243 K (Gür et al., 2005), O_4 (Greenblatt et al., 1997), NO_2 (Vandaele et al., 2002, 220 K), OClO (Bogumil et al., 2003, 293 K) and SO_2 (Bogumil et al., 2003, 273 K) were included in the retrieval. As in the case of the SO_2 fit, the SMR, a Ring spectrum, an inverse spectrum (calculated from the SMR) and a 5th order polynomial were also included in the BrO retrieval.

2.2 Alternative SO_2 retrieval in the case of very high SO_2 SCDs

During phases of explosive eruptions, very high SO_2 SCDs ($> 1 \times 10^{18}\,molec\,cm^{-2}$) can be observed in some parts of the detected volcanic plumes. For such cases, the atmosphere cannot be longer considered as optically thin for the standard SO_2 wavelength fit range (in this study 312.1–324 nm). The penetration of light in the plume becomes strongly wavelength dependent, resulting in low-biased SO_2 SCDs due to nonlinear effects. In extreme cases, only the outermost layers of the volcanic plume might be actually penetrated by the incident sunlight, and no light from inner parts of the plume or below is detected within the analysed wavelength range. However, this effect is usually reduced by light that

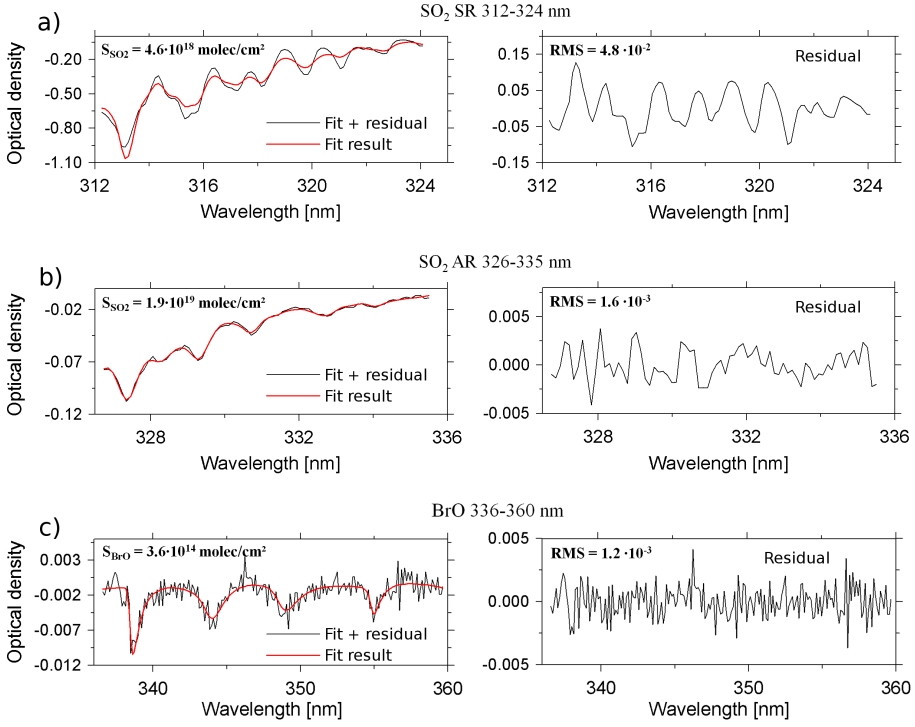

Fig. 1. Example of all three fit-scenarios, **(a)** SO_2 standard retrieval 312.1–324 nm, **(b)** SO_2 alternative retrieval 326.5–335.3 nm, **(c)** BrO retrieval 336–360 nm, for a GOME-2 pixel in the volcanic plume of Kasatochi on 9 August 2008 (21:05 UTC, centre coordinates 160.01° W 46.87° N). Left column: Fit results including the residual (black lines) and reference spectra (red lines) scaled according to the fit results (the resulting SCD (S) and root-mean-square (RMS) is also noted). Right column: corresponding residuals (please note expanded scales).

is scattered by aerosol particles, so that the SO_2 absorption signal is very weak, but not zero (Bobrowski et al., 2010).

Previous attempts to correct for this nonlinearity due to saturation effects relied on iterative model approaches (e.g. Yang et al., 2007, 2009; Richter et al., 2009), but such approaches are rather time consuming and need much computing power. Therefore, we decided to switch to an alternative evaluation fit range at slightly longer wavelength (326.5–335.3 nm), where the SO_2 absorption is weaker and, thus, the response of the resulting SO_2 SCDs is linear even at high SO_2 concentrations. In the following we refer to this alternative retrieval as the "SO_2 AR". For the SO_2 AR, again the O_3 cross sections from Gür et al. (2005, 223 K and 243 K) were used, as well as those for SO_2 (Bogumil et al., 2003, 273 K), the SMR, a Ring spectrum, an inverse spectrum (calculated from the SMR) and a 5th order polynomial. Although the sensitivity in the alternative wavelength range is clearly reduced in comparison to the standard fit range (the differential absorption cross section of SO_2 is about 2–3 orders of magnitude lower than for the SO_2 SR), this disadvantage is mostly compensated by the increased intensity of light towards longer wavelengths (λ) due to weaker absorption, less Rayleigh scattering (proportional to λ^{-4}) and, thus, higher AMFs. The evaluation at longer wavelengths in the case of large SO_2 SCDs, therefore, has the advantage that the signal-to-noise ratio is clearly increased, while the observed radiation has typically penetrated the whole plume. In Fig. 1, an example for both SO_2 DOAS retrievals (as well as for the BrO fit) is given for the volcanic plume of the Kasatochi eruption on 9 August 2008 (see also Fig. 11). While the SO_2 absorption features can be generally detected for the SO_2 SR, the residual shows significant systematic structures that are caused by the nonlinearity of the DOAS fit in cases of very strong SO_2 absorption (Fig. 1a). The resulting SO_2 SCD is $(4.6 \pm 0.3) \times 10^{18}$ molec cm^{-2} with a residual RMS of 4.8×10^{-2}. The fit results of the same GOME-2 pixel for the SO_2 AR in Fig. 1b clearly shows reduced systematic residual structures and a resulting SO_2 SCD of $(1.9 \pm 0.1) \times 10^{19}$ molec cm^{-2}, which is about 4 times higher than for the SO_2 SR. Additionally, the RMS of the residual is now about 40 times lower (1.2×10^{-3}) compared to the SO_2 SR. The BrO fit and residual of the BrO DOAS retrieval are additionally shown in Fig. 1c and indicate the presence of enhanced BrO SCDs in the volcanic plume. In order to use the advantages of the different evaluation schemes (high sensitivity of the SO_2 SR for small SCDs and no saturation of the SO_2 AR for high SCDs), we merged the SO_2 SR and the SO_2 AR to one "combined" SO_2 product. A detailed description how the results from both retrievals are merged for this combined SO_2 product will be given in Sect. 3.5.

3 Systematic study of volcanic BrO using GOME-2

The GOME-2 dataset was investigated for the simultaneous observation of volcanic SO_2 and BrO since the start of the regular measurements in January 2007 until the end of June 2011. Since SO_2 is usually the third most abundant gaseous species that is emitted by a volcano after H_2O and CO_2 (Schmincke, 2005), it has been used as a tracer in order to identify volcanic plumes in the satellite data. In total, 553 days with significantly enhanced SO_2 SCDs were found in the dataset, which were due to increased activity or eruptive phases of at least 37 volcanoes worldwide (the spatial proximity of several active volcanoes in some regions, e.g., the Kamchatka Peninsula, and the lack of local observations lead to the problem that the plume could not be unequivocally assigned to one specific volcano in some cases). Since enhancements of BrO columns in this study are only investigated for enhanced SO_2 columns, no statement can be made about the (probably unlikely) case, where SO_2 is below the detection limit, while enhanced BrO SCDs could be observed in a volcanic plume.

3.1 Automatic capturing of volcanic SO_2 plumes

In order to detect SO_2 plumes that are associated with increased activity or eruptive phases of volcanoes, the GOME-2 data was analysed using a newly developed detection algorithm that searches the dataset for conspicuously elevated SO_2 columns. Similar approaches have been developed during the last years in the course of operational early-warning systems for volcanic ash (e.g. Richter, 2009; SACS, 2012). Such early-warning systems provide rapid information to the aviation community about the location of a volcanic plume, which might compromise the safety of airplanes if they contain ash. Whereas these projects focus on near-real time early-warnings for volcanic ash plumes, the focus of our algorithm lies on the offline identification of volcanic plumes and especially the accurate extraction of SO_2-affected satellite pixels in order to compare the associated SO_2 SCDs with those of BrO in the GOME-2 dataset. Not only the reliable identification of volcanic plumes in the satellite data is needed, but also a more sophisticated correction for the non-volcanic BrO background signal in the vicinity of volcanic plumes.

3.2 Global maps with two days coverage

In a first step, the so-called "geometrical" SO_2 VCDs for all GOME-2 pixel were calculated from the SCDs by the use of geometrical airmass factors (AMFs):

$$\mathrm{VCD}_{\mathrm{i,geo}} = \frac{\mathrm{SCD}_{\mathrm{i}}}{\mathrm{AMF}_{\mathrm{i,geo}}} \quad (1)$$

$$\mathrm{AMF}_{\mathrm{i,geo.}} = \frac{1}{\cos(\theta_{\mathrm{i}})} + \frac{1}{\cos(\xi_{\mathrm{i}})} \quad (2)$$

where θ_{i} is the line-of-sight (LOS; nadir = 0°) and ξ_{i} is the solar zenith angle (SZA) during the measurement of satellite pixel i.

In the following, the data for two consecutive days were projected on gridded global maps covering two days at a grid resolution of 0.5° × 0.5°. These two days global maps (TDGM) differ from the commonly used layout for operational GOME-2 DOAS products, where all measurements of satellite orbits that had started within the regarded day (start time 00:00:00–23:59:59 UTC) are projected on a single global map (−90° N to +90° N and −180° E to +180° E). By using the TDGMs, we overcome a serious disadvantage of single day maps that is due to the occurrence of a temporal discontinuity in the illustration of data from satellites operating in sun-synchronous orbits. Figure 2a shows the GOME-2 satellite orbits for two consecutive days next to each other (day 1 on the right, day 2 on the left side). As the first and the last orbit of a single day is typically located at more than +105° E and extends up to +180° E and beyond, adjacent and/or overlapping pixels exhibit a time shift of up to 24 h (area between the light blue and green satellite orbits during day 1 and the green and dark red orbits during day 2 in Fig. 2a). Additionally, the orbits overlap at high latitudes (respectively low latitudes during arctic winter), so that also here time shifts of up to 10 h may occur between individual neighbouring satellite pixels. For the analysis of volcanic plumes that might be located at the edge of single day maps, the associated data can not be illustrated properly by simply sticking the maps of two consecutive days together, as another time shift of ∼24 h occurs at the intersecting region between day 1 and day 2. Therefore, the data in the TDGM was gridded in such a way that the chronology of the satellite orbits in direct succession is conserved in western direction (Fig. 2b). As the data has also been restricted to latitudes from −70° N to +70° N and SZA < 70° for this study, most overlapping pixels at high latitudes are skipped. Remaining overlapping pixels with a measurement time difference of more than ∼3.5 h (13 000 s) were discarded. By using the chronologically correct projection on the TDGM (that now extends from −540° E to +180° E in longitudinal direction), the temporal discontinuity can be avoided. Thus, the filtered satellite data within −180° E to +180° E now consequently contain all SO_2 fit results that were observed during the first regarded day (parts of the first 2 orbits at the eastern boundary of day 1 usually belong to the previous day), while most of the data within −540° E to −180° E contains the SO_2 columns for the following day. The most important advantages of the TDGMs are (1) being able to identify volcanic plumes close to the first or the last orbit of satellites in sun-synchronous orbits and (2) the ability to capture the complete plume, even if it extends beyond the common map boundaries in a westerly direction (< −180° E).

In order to prevent the detection of SO_2 events that are caused by non-volcanic emissions and/or measurement errors, the data for several areas are masked out. These include

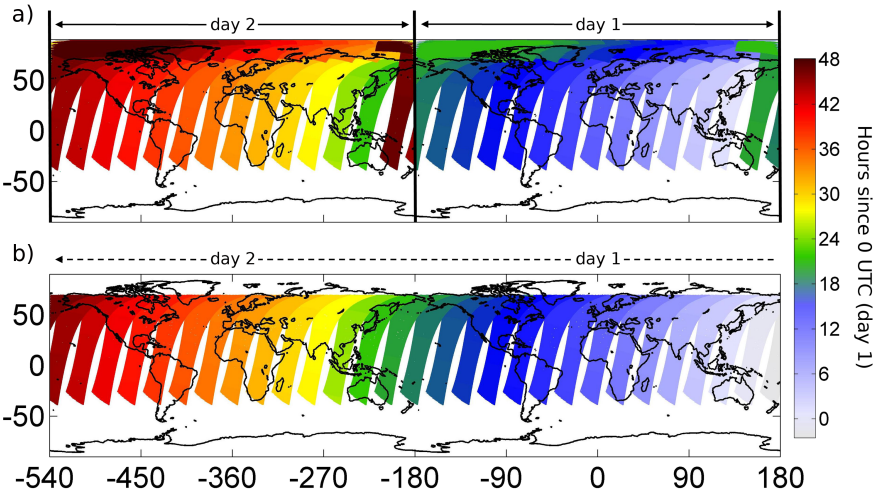

Fig. 2. (a) Two consecutive daily maps of GOME-2 satellite orbits as widely used in the scientific community (right: day 1, left: day 2). Due to an overlap of the first and the last orbit during one regarded day (area between light blue and green orbit for day 1 and green and dark red orbits during day 2), a temporal discontinuity of up to more than 24 h occurs. Additionally, overlapping pixels at high latitudes show a time shift of up to ∼10 h and another time shift of ∼24 h occurs at the intersecting region between day 1 and day 2. **(b)** Alternative global map layout for the maps with two days coverage. The chronology of satellite orbits in direct succession is now conserved in westerly direction. Measurements at more than ± 70° N and neighbouring pixels with a time shift >3.5 h are also filtered out.

Table 1. Areas where the GOME-2 data were excluded for the automatic detection of volcanic SO_2 plumes. The first three areas are affected by anthropogenic emissions of SO_2, whereas erroneous signals are detected over large parts of South America, where the deformation of Earth's magnetic field allows cosmic high-energy particles to create false signals in the detector of the satellite instrument (South Atlantic Anomaly).

name	reason	excluded area
Highveld plateau	anthropogenic emissions	[20°–35° S, 20°–35° E]
China	anthropogenic emissions	[20°–45° N, 100°–135° E] [30°–50° N, 130°–140° E]
Norilsk	anthropogenic emissions	[50°–70° N, 70°–110° E] [60°–70° N, 65°–70° E]
South Atlantic Anomaly (SAA)	cosmic particles	[10°–70° S, 10°–85° W] [0°–10° S, 10°–75° W] [20°–35° S, 0°–10° W]

in particular the greater area of Eastern China, Norilsk (Russia) and the Highveld plateau (South Africa), where anthropogenic SO_2 emissions can be regularly detected (caused e.g., by huge industrial coal plant and/or heavy metal smelter complexes), but also large parts of South America, where the satellite measurements are strongly influenced by the South Atlantic Anomaly (SAA) of the radiation belt. The excluded areas can be found in Table 1.

3.3 Volcanic plume extraction

After the data were projected on the TDGM, the SO_2 VCDs were corrected for an offset (usually caused by interferences with the O_3 absorption cross section and/or imperfect fitting of the Ring effect). For this purpose, the median in longitudinal direction for each grid pixel row (0.5°) was subtracted from the data. The offset corrected data were then subdivided into boxes of 5°×5° (10 × 10 grid pixels, for an example see Fig. 3). All boxes were investigated for a maximum SO_2 VCD of at least 5×10^{16} molec cm^{-2}, indicating that a box might contain a volcanic plume. This threshold was found to be well above the detection limit of the instrument and is consistent with typical SO_2 VCDs that are measured during strong degassing episodes and minor volcanic eruptions. Please note that, according to our data, the SO_2 detection limit has increased from approximately 1×10^{16} molec cm^{-2} in 2007 to more than 2×10^{16} molec cm^{-2} in June 2011 due to instrument degradation (for a detailed analysis of the impacts of the GOME-2 degradation on Level 2 products see

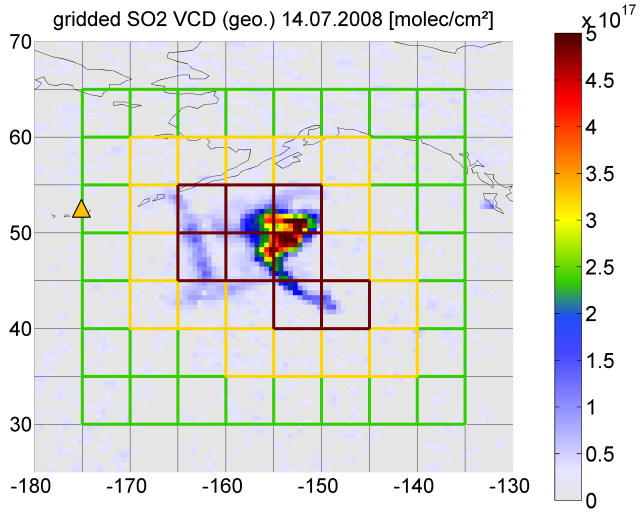

Fig. 3. Automatic detection of the volcanic SO_2 plume after the eruption of the Okmok volcano (orange triangle) on 14 July 2008. The red frames in the centre region highlight the detected SO_2 plume event boxes (PEBs) that were identified to contain parts of the volcanic plume. Neighbouring boxes are assigned to each specific PEB in order to capture also those parts of the volcanic plume where the VCDs were not sufficiently high to be identified as an individual PEB (yellow boxes). Finally, in order to get a reference area next to the captured SO_2 plume events, all non-SO_2 PEBs within another surrounding box that exceeded from $\pm 5°$ from the max/min latitudinal/longitudinal grid pixel position of the SO_2 PEB cluster were registered (green boxes).

also Dikty and Richter, 2011). However, since single erroneous measurements might sometimes also cause SO_2 VCD of comparable magnitude, all direct neighbouring grid pixels were additionally investigated using a second, lower SO_2 VCD threshold of 3×10^{16} molec cm^{-2}, to ensure the actual presence of an enhanced SO_2 VCD cluster inside the box area. Whenever at least 4 neighbouring grid pixels exceeded the second threshold, the box was assumed to contain at least parts of a volcanic SO_2 plume (see dark red boxes in Fig. 3). For each identified "SO_2 plume event box" (in the following abbreviated as "SO_2 PEB"), all directly neighbouring boxes were also assigned to this specific event in order to prevent losing parts of the volcanic plume where the VCDs were not sufficiently high to be identified as an independent SO_2 PEB (yellow boxes in Fig. 3). After all plume affected boxes had been determined, resulting clusters of SO_2 PEBs (red and yellow boxes) represent individual SO_2 plumes for the regarded days. In order to obtain a reference area next to the captured SO_2 plume events, all non-SO_2 PEBs within another surrounding box (that extends from $\pm 5°$ from the maximum/minimum latitudinal/longitudinal grid pixel position of the SO_2 PEB cluster) were registered (green boxes in Fig. 3).

To prevent the algorithm from capturing the same plume twice (as it always considers the data of two consecutive days), only SO_2 events that consist completely of satellite pixels recorded during the first regarded day or on the first *and* the following day were accepted for further investigation. Therefore, a SO_2 event that consists exclusively of measurements from the second of the two regarded days during an iteration of the algorithm was not captured until the subsequent iteration. This also means that the detection of a possible (but highly unlikely) case of a volcanic plume that encompasses the whole globe cannot be captured in its full extent using this approach. To the authors' knowledge, such an event has not occurred since the launch of GOME-2.

3.4 Non-volcanic background correction and plume pixel selection

Gridded satellite data are much easier to handle by the plume detection algorithm (see Sect. 3.3), because of the grid's regular geometry. Additionally, it has the advantage that background noise partly averages out during the gridding process, so that the misidentification of satellite measurements outside of a volcanic plume is prevented. However, for the further analysis of the volcanic plume events, the original GOME-2 ground-pixels associated with the registered grid boxes were regarded, as they represent the actual satellite measurements. In particular, individual satellite pixels have to be used for the correlation analysis between SO_2 and BrO, because the spatial patterns of both species are generally different.

For the detailed analysis of the BrO columns inside the detected volcanic SO_2 plumes and a possible correlation of the two species, the SCDs for SO_2 and BrO from the GOME-2 measurements need to be corrected for a non-volcanic offset. In contrast to the rough background correction process for the gridded satellite data in Sect. 3.3, the lat-/longitudinal offset was now corrected in a more sophisticated way. While the offset of SO_2 is mainly caused by the spectral interference with stratospheric ozone and/or the imperfect fitting of the Ring effect (see also Heue et al., 2011), the volcanic BrO signal is affected by the stratospheric BrO distribution (Theys et al., 2009b), which systematically depends on latitude (the BrO VCDs typically increase from $\sim 2 \times 10^{13}$ molec/cm^2 at equatorial regions up to $\sim 7 \times 10^{13}$ molec/cm^2 towards the poles, depending on season), but to a smaller degree also on longitude (small variations at the equatorial regions, but relatively strong variations of $\pm 2 \times 10^{13}$ molec/cm^2 for the VCDs at mid- and high latitudes). Additionally, extended areas in high latitudes might be affected by tropospheric BrO plumes that are formed, for example, at the sea ice surface during Artic spring in polar regions and can sometimes extend to latitudes of $\pm 70°$ N (Wagner and Platt, 1998). In a first step, the geometric AMF was used to convert SCDs to VCDs for both species (see also Sect. 3.3). This is a reasonable approach, as we are here mainly interested in correcting the influence of stratospheric BrO and O_3 to the resulting SCDs for BrO and SO_2, respectively. For the determination

of the latitudinal/longitudinal dependent offset of SO_2, a 2-dimensional spatial polynomial fit of 3rd degree was applied to the pixels from the reference area of the SO_2 PEB cluster (Fig. 3) and those pixels from the PEB cluster itself, whose SO_2 VCDs lay within 3σ of the reference area (and were, therefore, supposed to be located outside the volcanic plume):

$$SO_2VCD_{i,offset} \approx \sum_{m,n=0}^{3} a_{mn} \times x_i^m \times y_i^n \quad (3)$$

where a_{mn} are the fitted SO_2 offset VCDs at the centre coordinates x and y [°] of the satellite pixel i. All other satellite pixels within the PEB cluster (SO_2 VCD $> 3\sigma$ of the combined reference area) were now, in a first step, assumed to be part of the volcanic plume. Similarly, the corresponding BrO $VCD_{i,geo.}$ were approximated by a 2-dimensional polynomial of 4th degree (m, $n = 0,..,4$). The higher degree of the polynomial compared to the SO_2 background approximation was chosen because of the generally stronger spatial gradients of the BrO VCDs. It should be noted that the 2-D correction only removes a smooth background signal, but cannot completely remove non-volcanic BrO with strong spatial gradients. However, such events typically only occur at high latitudes. By subtracting the fitted polynomials from all VCDs (including the VCDs from the presumed volcanic plume pixels), we obtained the offset corrected geometrical vertical column densities VCD_i^*:

$$VCD_i^* = VCD_{i,geo.} - VCD_{i,offset} \quad (4)$$

All offset/background corrected pixels within the SO_2 PEB cluster were then once again checked for pixels whose VCD_i^* exceeded 3σ of the offset-corrected combined reference area. These pixels finally represented the identified volcanic plume.

Despite the different evaluation wavelength ranges, the AMF of the two species should only depend slightly on the altitude of the volcanic plume during most detected SO_2 events, with typical plume heights between 7 and 13 km (see Afe et al., 2004). However, the presence of volcanic ash might have an important influence on radiative transfer and, therefore, further information (e.g., about plume height and ash content) is necessary for a precise VCD calculation. As the focus of this study lies in the general ability of the GOME-2 instrument to detect BrO in addition to SO_2 during increased activity/eruptive phases of volcanoes (and the possible correlation between them), we simply reconverted the background corrected VCD_i^* into slant column densities SCD_i^* for the following investigations by multiplication with their $AMF_{i,geo.}$:

$$SCD_i^* = VCD_{i,geo.}^* \times AMF_{i,geo.} \quad (5)$$

3.5 Combination of SO_2 standard and alternative retrieval for major eruptions

Particularly for major volcanic events, we have to account for nonlinearities in the SO_2 retrieval, while for minor events, the standard retrieval is more appropriate. Thus, for the automatic plume extraction algorithm, both retrievals had to be combined. For all detected volcanic plumes where the maximum SO_2 SCD exceeded 1×10^{18} molec cm^{-2}, the results from the SO_2 AR were investigated for the same PEB clusters and associated reference areas as for the standard retrieval. The geometrical SO_2 VCDs from the AR were offset corrected in the same way as the VCDs from the SR (see Sect. 3.4). Again, all satellite pixels within the PEB cluster with a SO_2 VCD$>3\sigma$ of the offset corrected reference area were assumed to be part of the volcanic plume. Maps of the SO_2 plume were finally created by using the initial plume pixels from the SR, but all pixels with a SO_2 SCD $>1 \times 10^{18}$ molec cm^{-2} were replaced by the results from the AR, if the corresponding pixels were also found to be part of the plume after the background correction process (the choice of the SCD threshold is discussed in the Supplementary Material). In Fig. 4, the SO_2 plume from the Kasatochi eruption is shown for the 9th August 2008 (please note the logarithmic scale in Fig. 4a, b and d). While the maximum SO_2 SCD for the SR (Fig. 4a) is located in the southeastern part of plume (indicated by the small black star), it is shifted towards west for the AR (Fig. 4b). Additionally, the resulting SO_2 SCDs for the AR are now up to 5 times higher than for the SR, as can be seen in Fig. 4c, where the ratios of the resulting SO_2 columns from the different retrievals are shown for all pixels that were identified to be part of the plume in both evaluation wavelength regions. Results from both retrievals are finally combined in Fig. 4d. The plume's centre now looks much more structured than for the SR, where the central part of the plume mainly consists of a large homogeneous area, as most of the SO_2 SCDs seem to be scattered around 5×10^{18} molec cm^{-2} due to the saturation effect.

4 Results

The analysis of the GOME-2 measurements during the time period between January 2007 and June 2011 resulted in 772 SO_2 PEB clusters on 553 days, representing individual or at least completely isolated parts of volcanic plumes. Therefore, 33.7 % of all considered days (1642 days in total) showed signs of enhanced volcanic activity and/or eruptions in the satellite data. However, by looking at all captured events in the investigated satellite data, it becomes clear, that a general problem remains in identifying the source of some volcanic plumes in areas where several highly active volcanoes are located in close proximity. This is especially the case for the volcanoes on Kamchatka which houses about 29 active volcanoes. Whenever the origin of a volcanic plume

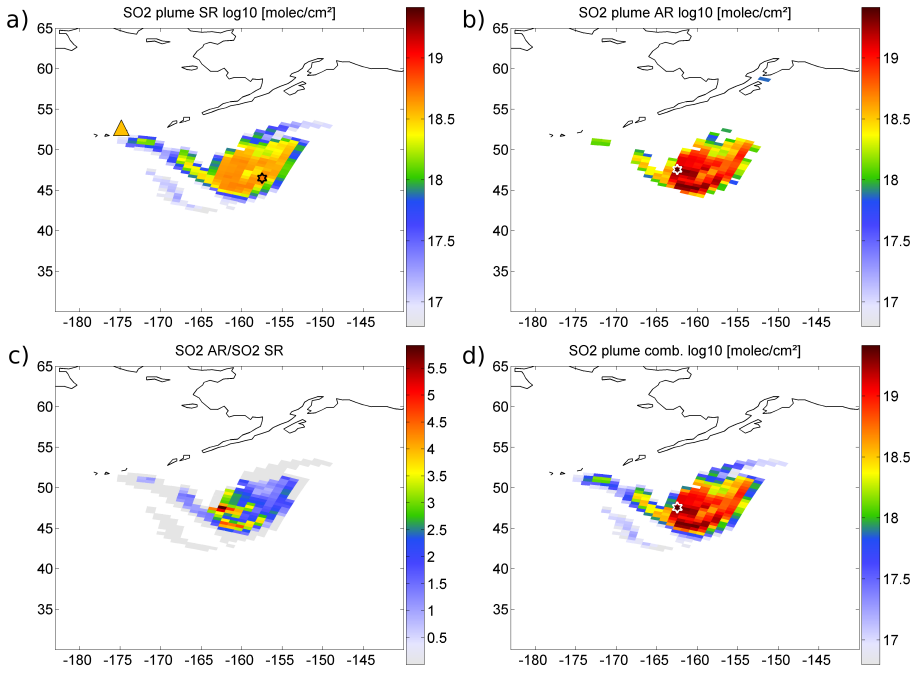

Fig. 4. Volcanic SO_2 plume as seen by GOME-2 on 9 August 2008 during the eruption of Kasatochi volcano. **(a)** SO_2 SCDs from the standard retrieval (312.1–324 nm), **(b)** SO_2 SCDs from the alternative retrieval (326.5–335.3 nm). While the maximum SO_2 SCD for the SR (5.2×10^{18} molec cm^{-2}) is located in the southeastern part of the plume (indicated by a black hexagon), it is now found to be shifted towards the west with a 5 times higher SCD (2.7×10^{19} molec cm^{-2}) in the AR (white hexagon). **(c)** Ratios between the SO_2 SCDs from the alternative and standard retrieval **(d)** The new SO_2 SCD product combines the results from both retrievals. Note the logarithmic scale in **(a)**, **(b)** and **(d)**.

could not clearly be identified, the most likely volcano is named. For that purpose, we cross-checked our data with online reports on the Global Volcanism Programme (GVP) website of the Smithsonian Institution (available under http://www.volcano.si.edu/reports/usgs/) and additionally with daily SO_2 maps from the Ozone Monitoring Instrument (OMI, http://so2.gsfc.nasa.gov/), the latter providing a more detailed spatial resolution of up to 13×25 km^2 (compared to 40×80 km^2 for GOME-2) and also daily global coverage. In Figs. 5 and 6, time series of the maximum VCDs* and corresponding integrated masses from our GOME-2 evaluation for SO_2 and BrO within all identified volcanic plumes are shown. Apart from many moderate eruptions and strong degassing volcanic events, several major eruptions are clearly visible in both time series, for example, the eruptions of Okmok (Aleutian Islands, July 2008), Kasatochi (Aleutian Islands, August 2008), Sarychev (Kuril Islands, June 2009), Merapi (Indonesia, November 2010), Grímsvötn (Iceland, April 2011) and Nabro (Eritrea, June 2011). For the BrO VCDs*, the time series indicates the presence of volcanic BrO during some of the monitored SO_2 events. While the maximum BrO VCD* for most of the volcanic events is around 2.5×10^{13} molec cm^{-2}, the VCDs* during several eruptions show much higher values. However, only some of these events show significantly enhanced VCDs, meaning that the VCD exceeds twice the fit error (events indicated in blue). Although the BrO masses in Fig. 6 appeared to be enhanced for some eruptions where no significantly enhanced maximum BrO VCD was found (e.g., Okmok in July 2008), the corresponding total mass errors constitute more than 50 % of the total mass and are, therefore, not reliable (indicated in red).

In the following, several volcanic eruptions will be presented and discussed in more detail in order to investigate the different SO_2 to BrO relationships that have been observed. For this purpose, we will focus on some of those volcanic plumes where the BrO VCD^*_{max} were clearly above the detection limit (exceeding 5×10^{13} molec cm^{-2}) and, therefore, indicate the presence of volcanic BrO. This includes the eruptions of BZ – Bezymianny (Kamchatka Peninsula) in May 2007, ET – Mt. Etna in May 2008, KS – Kasatochi volcano in August 2008, DL – Dalaffilla (Ethiopia) in November 2008, RD – Redoubt (Alaska) in March/April 2009, SA – Sarychev (Kuril Islands) in June 2009, EY – Eyjafjallajökull (Iceland) in April/May 2010 and NB – Nabro volcano in June 2011 (see labelled time periods in Figs. 5 and 6 and Table 2, respectively). The sequence of selected examples starts with volcanic plumes which show a high correlation and continues with examples of decreasing degree of correlation. All examples are examined for linear correlation between the two

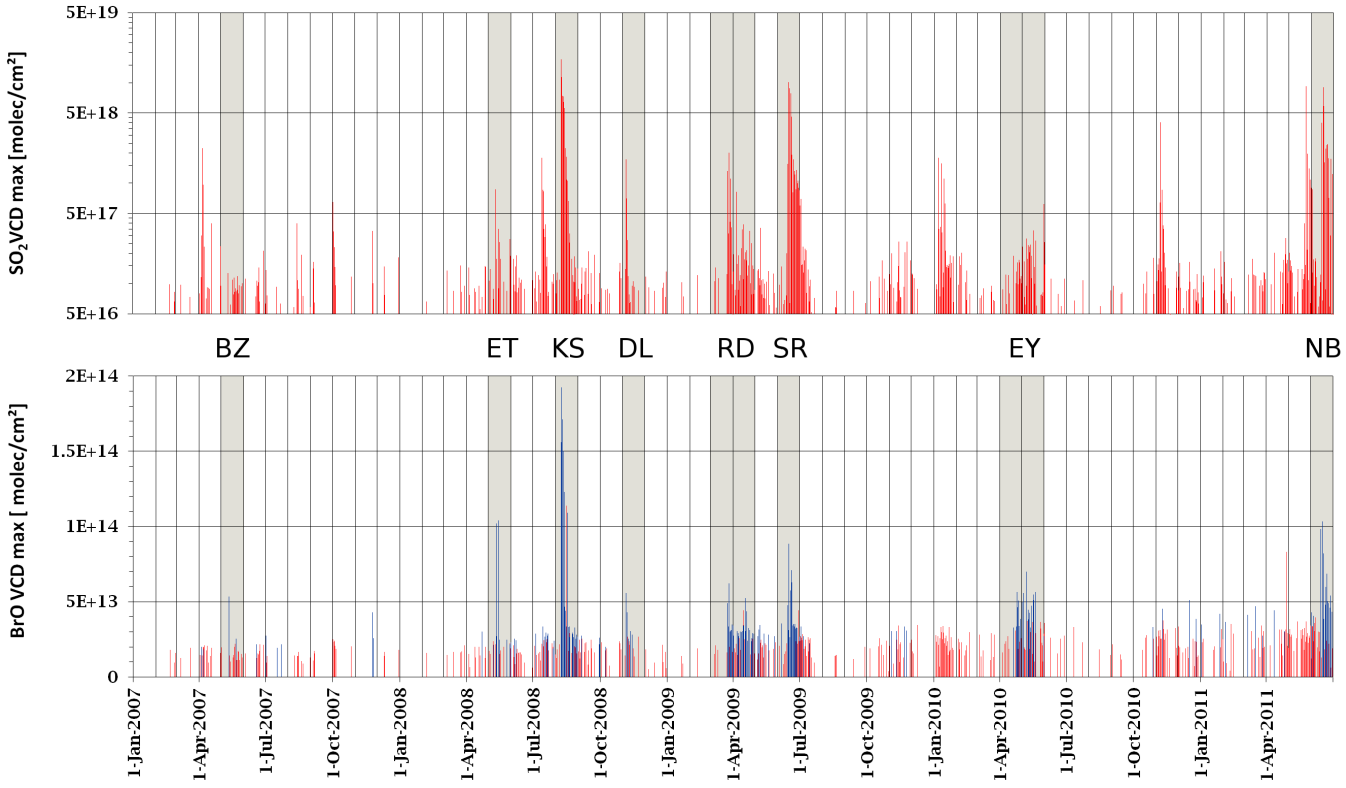

Fig. 5. Time-series of maximum GOME-2 SO_2 and BrO VCDs* (geometrical AMF and background corrected) within all individual volcanic plumes, captured by the automatic plume detection algorithm between January 2007–June 2011. For several SO_2 plume events, the maximum BrO VCDs* are significantly elevated at the same time (please note the logarithmic scale for SO_2). This is, in particular, the case for the eruptions during the highlighted periods (BZ – Bezymianny, ET – Etna, KS – Kasatochi, DL – Dalaffilla, RD – Redoubt, EY – Eyjafjallajökull, NB – Nabro). The BrO VCDs that were larger than two times the associated fit error are highlighted in blue.

Table 2. Examples for the abundance of volcanic BrO that are presented in Sect. 4.1-4.6.

label	volcano	date	section	figure
ET	Etna	14 May 2008	Sect. 4.1	Fig. 7
BZ	Bezymianny	11/12 May 2007	Sect. 4.2	Fig. 8
DL	Dalaffilla	4 November 2007	Sect. 4.3	Fig. 9
NB	Nabro	16 June 2011	Sect. 4.4	Fig. 10
KS	Kasatochi	9 and 11 August 2008	Sect. 4.5	Figs. 11–12
SR	Sarychev	15/16 June 2009	Sect. 4.6	Fig. 13

species by applying a bivariate linear fit (Cantrell, 2008) to the SO_2 and BrO SCDs* of the identified plume pixels. In addition, the ratio of integrated molecules within the plume is given in the correlation plots, which might be more meaningful for cases where no correlation could be observed. For all BrO/SO_2 ratios, corresponding errors were calculated by taking the individual SO_2 and BrO fit errors into account. The systematic errors (especially radiative transfer effects), however, are supposed to (mainly) cancel out by taking the BrO/SO_2 ratio and are, therefore, neglected.

4.1 Etna (14 May 2008) – ET

Being one of the most active volcanoes in the world and easily accessible, Etna is one of the most frequently monitored volcanoes. According to reports from the Istituto Nazionale di Geofisica e Vulcanologia, sezione di Catania (INGV-CT), a new eruptive fissure opened on Etna's upper east side on May 13, after several months of seismic unrest (Smithsonian, 2007–2011). Figure 7 shows the volcanic plume during the eruption on 14 May 2008 (labelled ET in Fig. 5). The SO_2 and BrO SCDs* of the whole regarded area (including the plume and reference area) can be seen in Fig. 7a

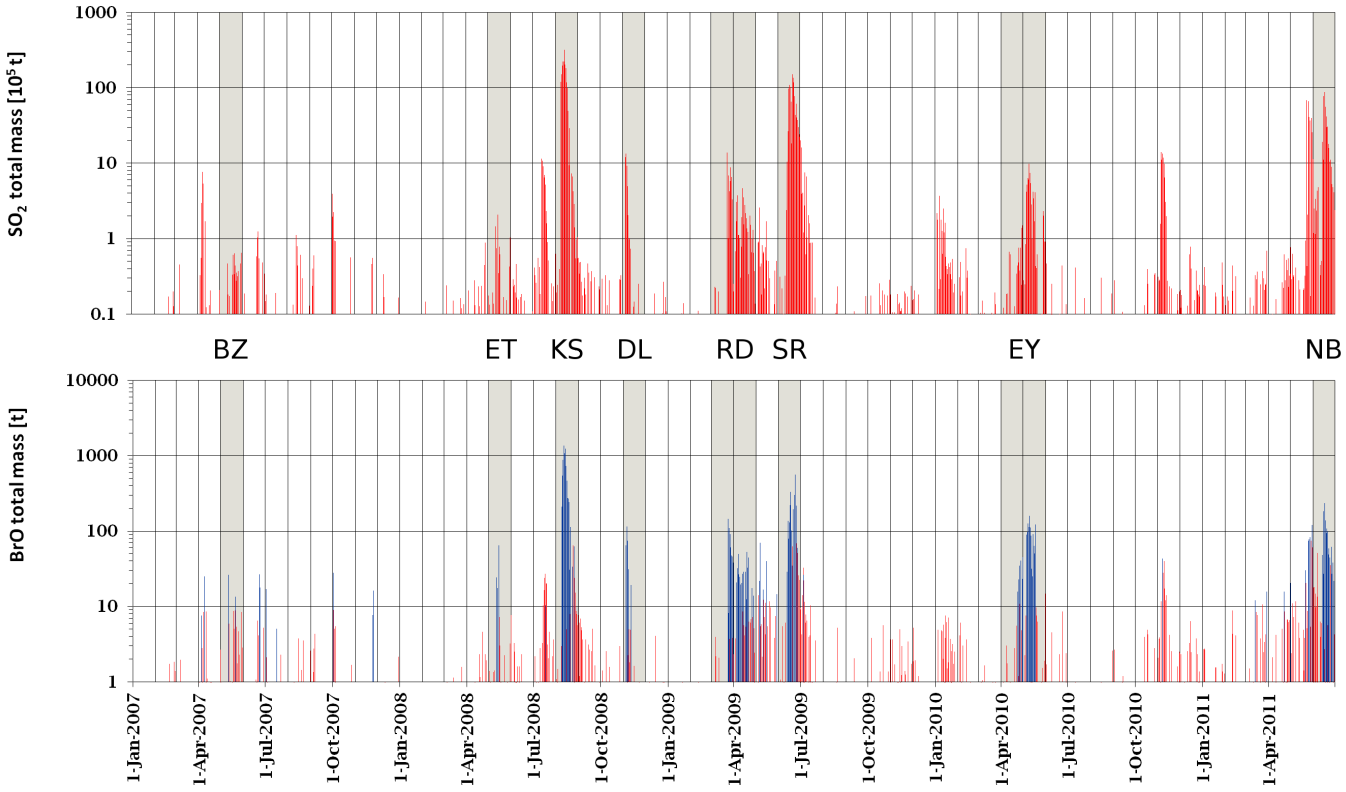

Fig. 6. Time-series of integrated total SO_2 and BrO masses for all investigated volcanic plumes between January 2007–June 2011. Like for the maximum VCDs in Fig. 5, also the integrated BrO masses are significantly enhanced at the same time as the number of SO_2 molecules. For many days, the detected BrO mass is significant (> two times the corresponding error), as indicated in blue. Please note the logarithmic scales.

and c, respectively. Figure 7b and d show only the satellite pixels where the SO_2 VCDs* were larger than $3\sigma^*$ (with σ^* the standard deviation of the reference area). The corresponding correlation plot (Fig. 7e) shows a clear linear correlation between the two species with r^2=0.7 and a fitted mean BrO/SO_2 ratio of $(2.7 \pm 0.2) \times 10^{-4}$. It is interesting to mention, that the location of the SO_2 SCD^*_{max} corresponds to the location of the BrO SCD^*_{max}. Another eruption at the Southeast Crater of Mt. Etna on 10 May 2008 (Bonaccorso et al., 2011) showed similar behaviour, with a linear correlation between the two species and a BrO/SO_2 ratio of almost 1×10^{-4}.

On closer examination, it can further be seen that a small part of the plume close to the volcano shows enhanced BrO SCDs in absence of enhanced SO_2 and is, therefore, not included in the BrO/SO_2 analysis. According to a visual inspection of all volcanic plumes investigated within the scope of this paper, this is a one-time-only event. As the corresponding BrO SCDs are close to the BrO detection limit, a clear verification of the enhancement remains difficult.

4.2 Bezymianny/Kliuchevskoi (11/12 May 2007) – BZ

The Bezymianny volcano is one of 29 active volcanoes on the Kamchatka Peninsula. The volcano was moderately active throughout the whole year 2007, interrupted by some small explosions in May and October-December. Figure 8 shows the trace gas distribution after such an explosion of the volcano on 11/12 May 2007 (labelled BZ in Fig. 5). In Fig. 8a, the background corrected volcanic SO_2 plume after the explosion of Bezymianny (indicated by the orange triangle) can be seen over the Kamchatka Peninsula. Below (Fig. 8c), the BrO SCDs* are shown for the same area, indicating the presence of enhanced BrO columns in the same area as the enhanced SO_2 SCDs*. Like for the previous example of Mt. Etna, Fig. 8b and d show only the satellite pixels that were assumed to contain the volcanic plume (SO_2 VCDs* $>3\sigma^*$). These pixels were used for the correlation plot (Fig. 8e), with a correlation coefficient $r^2 = 0.62$ and a resulting mean BrO/SO_2 ratio of $(5.1 \pm 1.0) \times 10^{-4}$.

Due to the close spatial proximity of Bezymianny to the Kliuchevskoi volcano (∼10 km), we can not be entirely sure that the observed volcanic plume came from Bezymianny alone, as Kliuchevskoi showed also increased activity at the time of the measurements according to reports of the

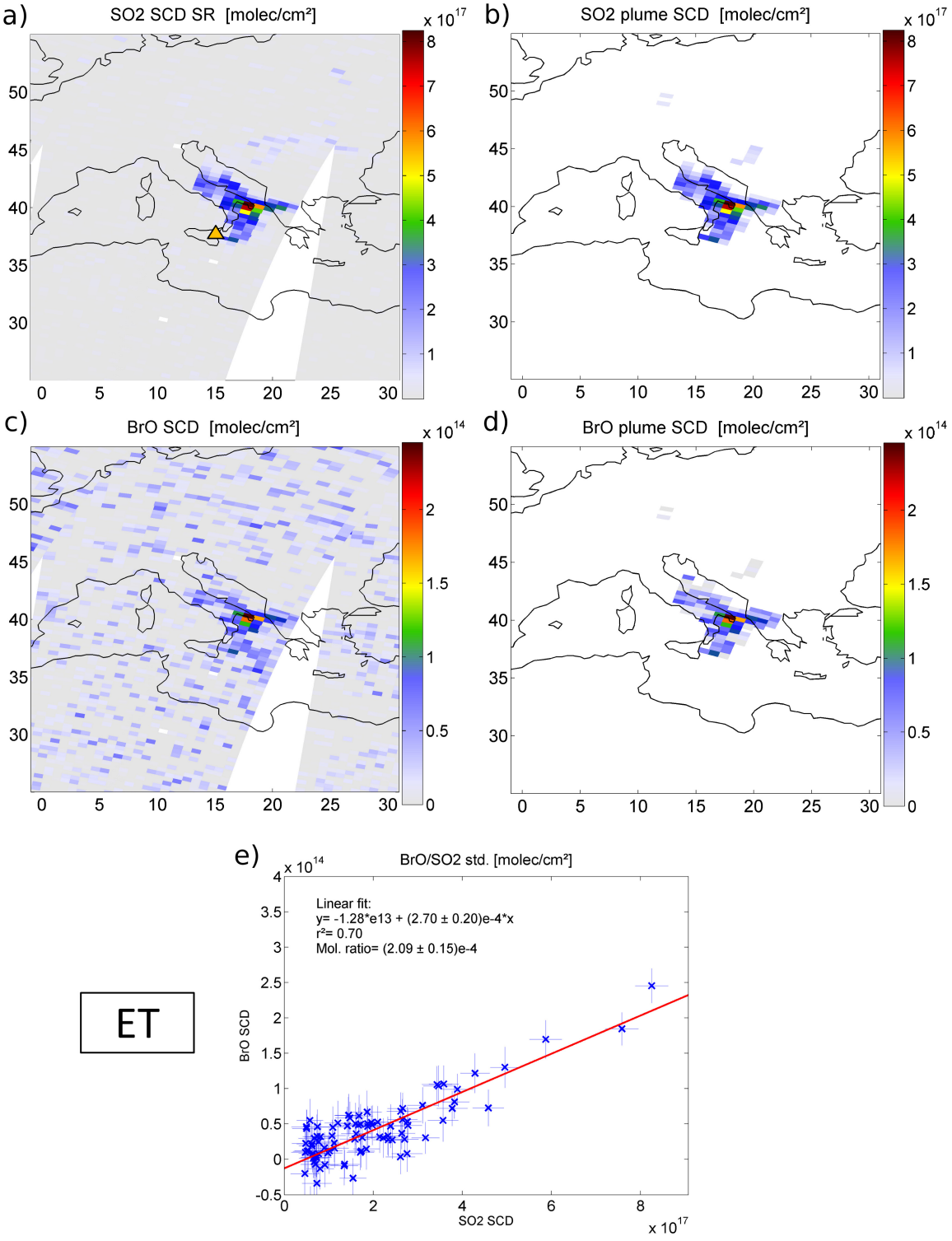

Fig. 7. SO_2 and BrO SCDs during an eruptive phase of Mt. Etna on 14 May 2008. The SCDs for SO_2 and BrO (**a** and **c**) show that the BrO SCDs were clearly enhanced in the vicinity of the SO_2 plume and even have a similar distribution. **(b)** and **(d)** show only those satellite pixels, that are supposed to represent the volcanic plume (SO_2 VCD$^* > 3\sigma^*$). The correlation plot for the identified plume pixels **(e)** shows a linear relationship between the two species ($r^2 = 0.7$) and a fitted mean BrO/SO_2 ratio of $(2.7 \pm 0.2) \times 10^{-4}$.

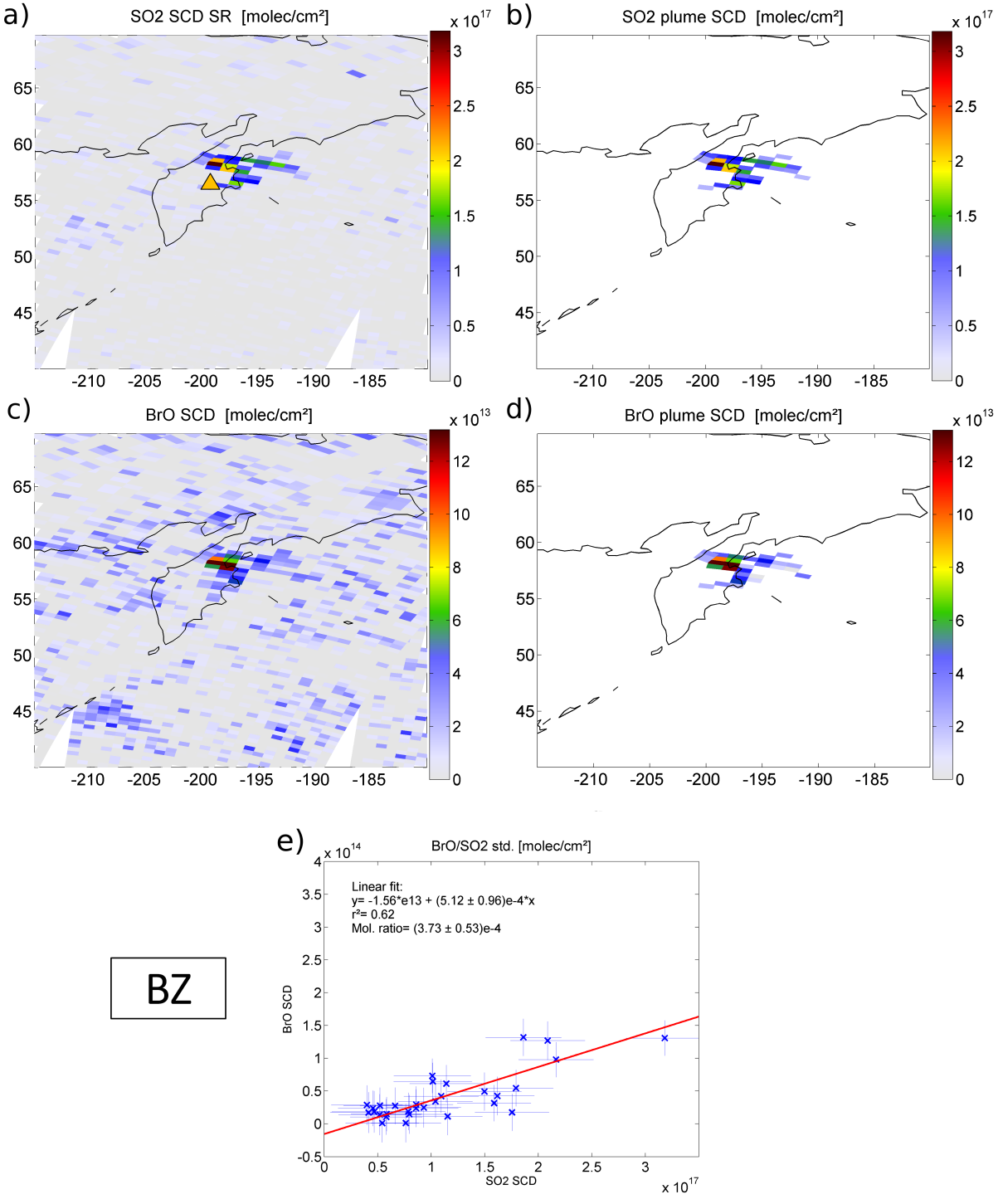

Fig. 8. SO_2 and BrO SCDs during an eruptive phase of Bezymianny volcano (Kamchatka Peninsula) on 11/12 May 2007. Next to the SO_2 plume **(a)**, volcanic BrO was present, as the BrO SCDs are clearly enhanced in the vicinity of the SO_2 plume **(c)**. The satellite pixel with SO_2 SCDs $> 3\sigma$ of the reference area are shown in **(b)** and **(d)** for both species. The correlation plot for the identified plume pixels **(e)** shows a linear relationship between the two species ($r^2 = 0.62$) and a fitted mean BrO/SO_2 ratio of $(5.12 \pm 0.96) \times 10^{-4}$.

Kamchatka Volcanic Eruption Response Team (KVERT). However, as seismic data suggested an explosive eruption of Bezymianny shortly before the satellite measurements (Smithsonian, 2007–2011), it seems most likely that the major part of the visible plume originated from Bezymianny with minor parts from Kliuchevskoi (see also the KVERT webpage for detailed activity reports on http://www.kscnet.ru/ivs/kvert/updates/).

4.3 Dalaffilla (4 November 2008) – DL

On 3 November 2008, an eruption of the Dalaffilla volcano in Ethiopia's Afar region produced an extensive plume of SO_2, which was rapidly transported in a northeastern direction towards the Arabian Peninsula and reached the western part of China after two days. While the GOME-2 instrument was able to track the SO_2 plume for about 10 days, BrO was only clearly detected on the very first day after the eruption on November 4, when the plume was also seen for the first time by the satellite instrument (labelled DL in Fig. 5). Figure 9a shows that the SO_2 plume can be separated into two main parts, one with rather high SO_2 SCDs* over the southeastern side of the Arabian Peninsula, the other one with lower SO_2 SCDs* further in the north west. In contrast to these findings, the BrO SCDs* (Fig. 9c) were only significantly enhanced in the northwestern part of the extracted SO_2 plume (Fig. 9b) and in a long band towards the Persian Gulf. The consideration of all identified SO_2 plume pixels, therefore, leads to no clear linear correlation between the two species, but already indicates that such a correlation might be present in some parts of the plume. If we limit the focus to the plume pixels around the region with the enhanced BrO SCDs* (indicated by the red polygon in Fig. 9b and d), a linear correlation between the SO_2 and BrO SCDs* is found, with r^2=0.54 and a mean fitted BrO/SO_2 ratio of $(6.4 \pm 0.8) \times 10^{-5}$. Please note the smaller total molecule ratio of $(4.0 \pm 0.3) \times 10^{-5}$ due to the consideration of all plume pixels. It seems remarkable that no enhanced BrO SCDs* can be found in the southeastern part of the plume, while the maximum SCDs* of SO_2 were observed within this area. Possible reasons for this non-uniform distribution of the enhanced BrO SCDs* will be discussed in Sect. 6.

4.4 Nabro (16 June 2011) – NB

Announced by an earthquake swarm on 12 June 2011, the first recorded eruption of the Nabro volcano (Eritrea, Africa) started one day later in the early morning of June 13 (labelled NB in Fig. 5). As the Afar Triangle area in Southern Eritrea is barely populated, first observations of the eruption by eye witnesses did not occur until the late evening (Smithsonian, 2007–2011), while several satellite instruments (namely GOME-2, SCIAMACHY, OMI, the Atmospheric Infrared Sounder – AIRS – and the Infrared Atmospheric Sounding Interferometer – IASI) were already able to monitor the plume's propagation towards Northern Egypt for about 2,000 km during the whole day (SACS, 2012). On the 16th June, the GOME-2 SO_2 measurements (Fig. 10a) show that while the plume front had been transported to Western China the volcano continued to emit significant amounts of SO_2. From the BrO retrieval (Fig. 10c), enhanced SCDs* can only be seen clearly within the area of the highest SO_2 SCDs* that occur about 600–700 km from the volcano. Whenever the volcanic plume was captured by the GOME-2 measurements in the course of the eruption, similar behaviour was found for all days with significantly enhanced SO_2 SCDs* in June. Taking all SO_2 plume pixels into account (Fig. 10b and d) yields a poor correlation coefficient ($r^2 = 0.29$) of the linear fit, which results mainly from the majority of pixels where the SO_2 SCDs* were significantly enhanced while the BrO SCD* were not, causing a strong scattering around zero at low SO_2 slant column densities (Fig. 10e – blue crosses). By restricting the data to the area with clearly enhanced BrO SCDs (indicated by the red shape in Fig. 10b and d), the r^2 value increases to 0.49 (Fig. 10e – red crosses). The rather low fitted mean BrO/SO_2 ratio of $(1.3 \pm 0.1) \times 10^{-5}$ suggests that the main reason for the apparent absence of BrO in the aged plume might be that the BrO SCDs no longer exceeded the instruments' detection limit. In addition, the conversion of BrO into other bromine species might also play a role.

Another possible reason for the different distributions of both species might be that the plume close to the volcano consists of two layers at different altitudes (Theys et al., 2012). Most of the enhanced BrO SCDs belong to a plume layer that is located at lower altitudes (4–5 km) and extends towards southern direction, while the dominating part of the plume is located at 10–12 km and no BrO was detected. A precise separation of both plume layers remains difficult, especially in the overlapping area close to the volcano. However, the data were reanalysed for the very southern part of the plume (where an overlap with the plume layer at higher altitudes could be excluded), but no significant differences for the BrO/SO_2 ratio (respectively the correlation plot) were found in comparison to the consideration of the whole area with enhanced BrO SCDs. The plume composition at different altitudes might vary due to different volcanic processes, such as energetic lava fountains during strong explosions (for the plume at higher altitudes) and residual degassing of lava flows (plume at low altitudes). Such mechanisms are known to produce differences in the ratios of SO_2 and halogen species like HCl or HF (e.g. Burton et al., 2003; Bobrowski and Giuffrida, 2012; Ohno et al., 2013). These differences might also affect the BrO/SO_2 ratio.

4.5 Kasatochi (9 and 11 August 2008) – KS

After an increase in the seismic activity during the first days of August 2008, at least five distinct explosions occurred at the Kasatochi volcano in the afternoon of 7 August

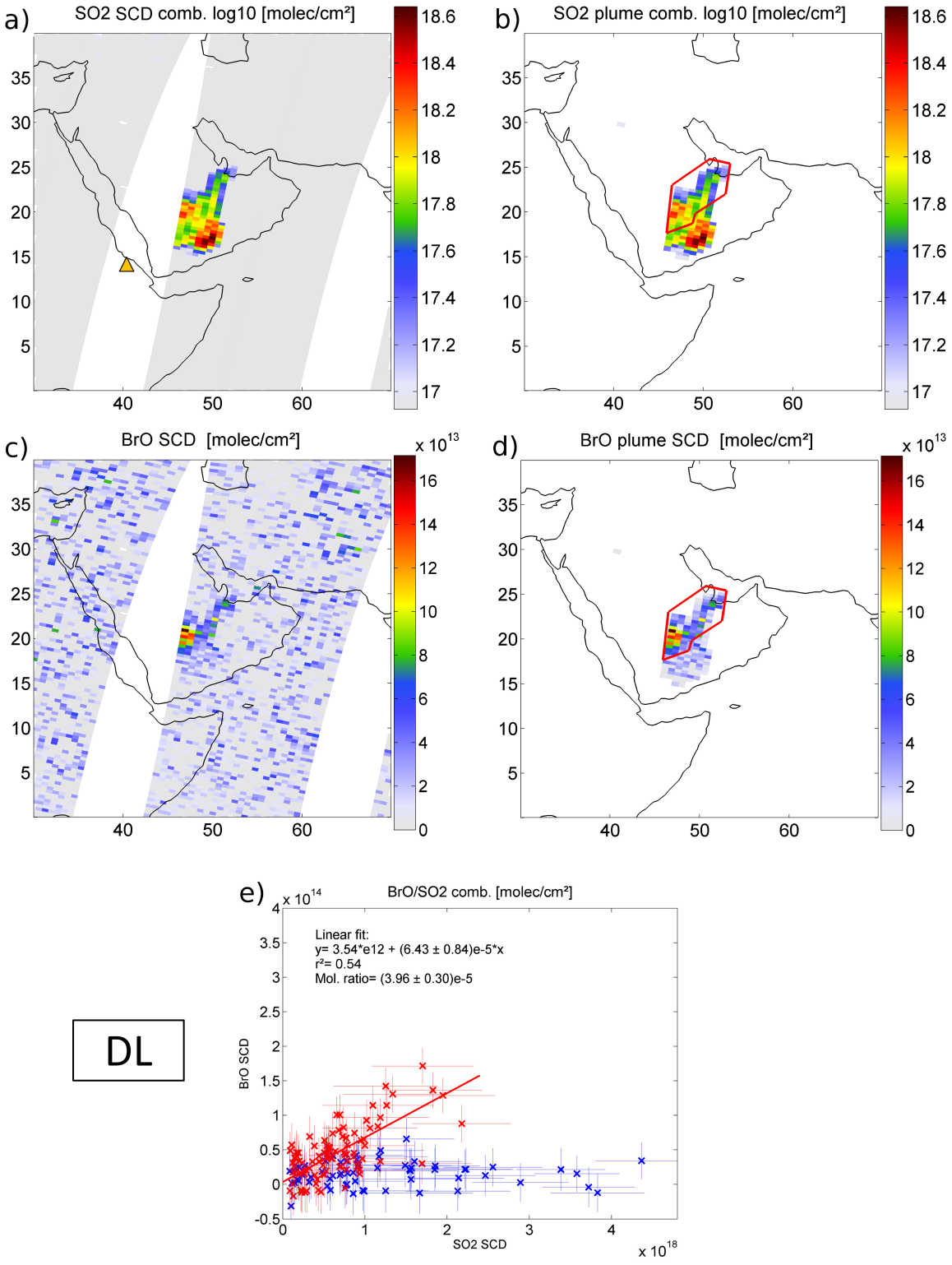

Fig. 9. GOME-2 measurements of SO_2 and BrO SCDs after the eruption of the Dalaffila volcano on 4 November 2008. The SO_2 plume is separated into two main parts and can be clearly seen in **(a)** the combined SO_2 retrieval (please note the logarithmic scale). In **(b)**, only the significantly enhanced SO_2 SCDs*>3σ^* are shown. Enhanced BrO SCDs* are only located in the northwestern part (**c** and **d**). A linear correlation can only be seen for a restriction to this area, which is indicated by the red polygon in the maps and the red crosses in the correlation plot **(e)**. Blue crosses represent measurements outside the restriction area. The r^2 is then 0.54 with a fitted mean BrO/SO_2 ratio $\sim 6.4 \times 10^{-5}$.

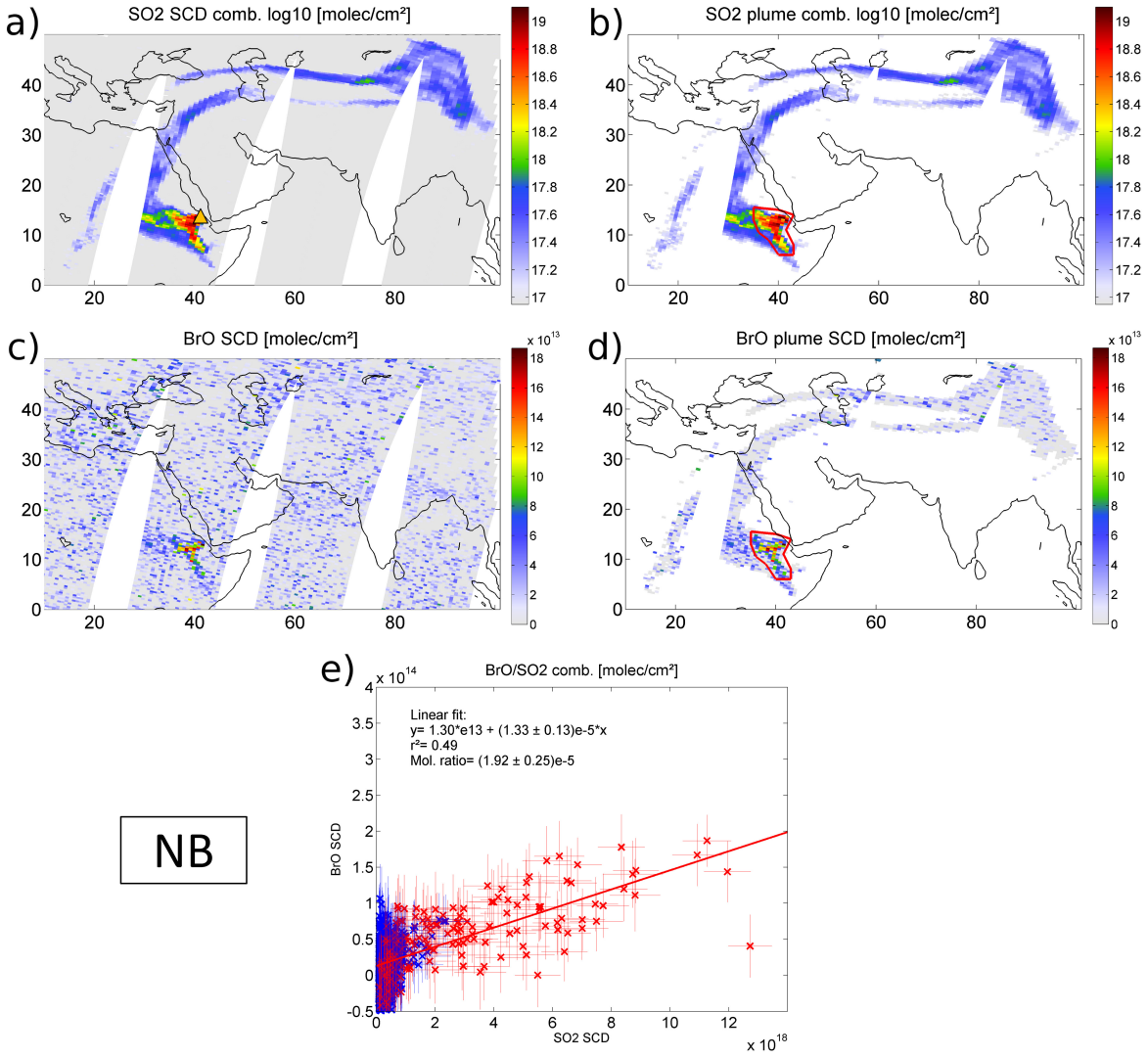

Fig. 10. SO_2 and BrO SCDs during the eruption of the Nabro volcano (Eritrea) on 16 June 2011. The SO_2 plume spreads several thousands of kilometres from the volcano towards East Asia (**a** and **b**). The enhanced BrO SCDs* appear only relatively close to the volcano (in the same area where the highest SCDs* of SO_2 are detected) and show a similar distribution (**b** and **d**). While the r^2 from the linear fit for *all* identified plume pixels (blue and red crosses) is rather low (0.29), the restriction to the area with clearly enhanced BrO SCDs* results in $r^2 = 0.49$ (area is indicated by the red polygon in **(c)** and **(e)**; corresponding SCDs* by red crosses in the correlation plot **(e)**). The fitted mean BrO/SO_2 ratio is low compared to other eruptions with $\sim 1.3 \times 10^{-5}$.

(Waythomas et al., 2010). While the first two explosions produced large ash-poor gas-charged plumes, the third one was relatively ash-rich and emitted massive amounts of SO_2, which reached the lower stratosphere at about 18 km. The two remaining explosions were of minor intensity and only detected by seismic stations (Neal et al., 2011).

The SO_2 plume was detected the first time on 8 August by several satellite instruments (including GOME-2, SCIAMACHY and OMI) and further tracked for at least one month while the plume circled the globe (labelled KS in Fig. 5). The observation of an extensive BrO cloud in the vicinity of the SO_2 plume by GOME-2 was reported by Theys et al. (2009a). In contrast to the SO_2 plume, the BrO could only be clearly tracked for about one week. Yet, the GOME-2 observations of the Kasatochi plume provide so far the longest continuous measurements of a single volcanic BrO plume since the first ground-based measurements of volcanic BrO (Bobrowski et al., 2003). The absolute BrO VCDs* during the first days of the eruption ($\approx 2 \times 10^{14}$ molec cm^{-2}) were about a factor of 2–3 larger than for the cases discussed in Sects. 4.1–4.4. While all previously presented eruptions of Mt. Etna, Bezymianny, Dalaffilla and Nabro showed similar spatial distributions for BrO and SO_2 and a linear correlation (at least in parts of the plume), the eruption of Kasatochi showed only a roughly similar spatial pattern between the two observed species, with growing differences in

the distribution of the two species while the initial plume was transported towards east. Figure 11 shows the volcanic plume on the second day of the GOME-2 observations (9 August 2008). While the enhanced BrO SCDs* (Fig. 11c and d) are located in the same area as the captured SO_2 plume pixels (Fig. 11a and b), the spatial distribution for BrO appears more circular in shape than the SO_2. The location of the maximum SCDs* also differs for both species. The maximum SO_2 SCDs* are located in the southern region of the plume, while the maximum BrO SCDs* can be found in the western and eastern part. The correlation plot (Fig. 11e) shows a positive correlation between the species ($r^2 = 0.24$), but also a large scatter in the BrO SCDs* with increasing SO_2 SCDs*. For more complex cases like the Kasatochi eruption, the ratio by dividing the total number of molecules is probably better suited to give an estimate of the mean obtained BrO/SO_2 ratio and was found at $(2.51 \pm 0.04) \times 10^{-5}$.

In Fig. 12, the plume is shown 2 days later on 11 August 2008. Whereas the main plume has moved towards the Canadian west coast, several branches reach out from the plume centre in a southwestern and northeastern direction (Fig. 12a). The clearly enhanced BrO SCDs* are located around the centre region of the SO_2 plume, but the distribution of the trace gases within this area is different (Fig. 12c). The map of the extracted plume pixels for BrO (Fig. 12d) in comparison to those for SO_2 (Fig. 12b) indicates that most of the BrO seems to be twisted around the plume centre containing the highest SO_2 SCDs*. Especially the BrO SCDs* at the location of the highest SO_2 SCDs* are not as high as for the surrounding area. This can also be seen in the correlation plot (Fig. 12e), where the BrO SCDs* are linearly correlated up to SO_2 SCDs* $< 5 \times 10^{18}$. For higher SO_2 SCDs*, the BrO columns appear to level out around 2.5×10^{14} molec cm^{-2}. One possible reason for such a behaviour might be, that the plume centre was not yet entirely mixed with ambient ozone-rich air after sunrise at the time of the GOME-2 measurements. Generally, the differences between the SO_2 and BrO distributions during the eruption may also be partly caused by differences in the injection profiles of the individual explosions.

4.6 Sarychev (15/16 June 2009) – SR

The eruption of the Sarychev volcano (Kuril Islands, Russia) in June 2009 is another example of a complex BrO/SO_2 relationship as seen in the case of Kasatochi (labelled SR in Fig. 5). According to the Sakhalin Volcanic Eruption Response Team (SVERT), the first signs of an eruption were found in satellite observations acquired on 11th June (Smithsonian, 2007–2011). After the main phase ended on the 16th June, several weaker eruptions occurred in the following 2 weeks. In Fig. 13a, the plume for the combined SO_2 retrieval can be clearly seen for the 15th/16th of June. The volcano (indicated by the orange triangle in Fig. 13a) is located on the island Matua (48°5′30″ N, 153° 12′0″ E), and surprisingly, the SO_2 plume spreads in opposing directions, westward and eastward from the volcano (Fig. 13a and b). By looking at the corresponding maps for BrO (Fig. 13c and d), one can see that enhanced BrO SCDs* were only detected in a relatively small region in the western part of the plume for that day (other days during the eruption showed also different BrO/SO_2 patterns; see the Supplement). The correlation plot (Fig. 13e), therefore, leads to an r^2 value close to zero from the bivariate linear fit ($r^2 = 0.01$). Although a linear branch seems to be present in the plot at lower SO_2 SCDs* (like for the Dalaffilla eruption described in Sect. 4.3), a restriction to the area of the satellite pixels with elevated BrO SCDs* did not lead to a clearer result regarding a linear correlation between both species. Additionally, the GOME-2 UV Absorbing Aerosol Index (AAI) for the regarded day can be seen in Fig. 14a (Penning de Vries et al., 2009). The AAI is a semi-quantitative measure of aerosols that absorb UV radiation. It is most sensitive to elevated layers of absorbing particles such as smoke, mineral dust and volcanic ash and depends mainly on aerosol optical thickness, single-scattering albedo and altitude of the aerosol layer (e.g. Herman et al., 1997; Torres et al., 1998; Graaf et al., 2005). As one can see in the map, volcanic ash seems to have been present almost in the entire extent of the volcanic SO_2 plume, while the most enhanced values occur in western direction from the volcano. This suggests, that there might have been an ash-rich explosion shortly before the GOME-2 measurements, of which the plume was mainly transported westwards.

In a case study, we tried to reproduce the volcanic plume's propagation by trajectories from the Hybrid Single Particle Lagrangian Integrated Trajectory Model (HYSPLIT – see Draxler and Rolph, 2012; Rolph, 2012). For the simulation of the plume's spreading, we used the starting times for individual explosions, as reported by Levin et al. (2010), who used satellite images of the geostationary Multi-functional Transport Satellites (MTSAT) during the eruptive phase of the volcano in order to reconstruct the main explosion events. In total, 23 individual explosions were found between the 13th and the 22th June, with 13 of them being powerful enough to reach more than 6 km altitude. The multitude of explosions also points out the difficulties of the determination of a mean BrO/SO_2 ratio for such major eruptions, as several overlapping plumes at different altitudes (and, therefore, different ambient conditions) might be present in the observed satellite data, which only represent a 2-dimensional projection of the plumes at different altitudes. Additionally, the plume's chemical composition may change significantly in the course of an eruption. In case of the example shown in Fig. 13, we used the starting time of the five strongest explosions within the two days prior to the satellite measurements for the calculation of the forward trajectories (19:00 UTC on 14 June; 01:00 and 09:00–11:00 UTC on 15 June), all of them with reported top heights of more than 10 km. The trajectories for all explosions were calculated for starting heights between 5–20 km at the location of the volcano until the GOME-2

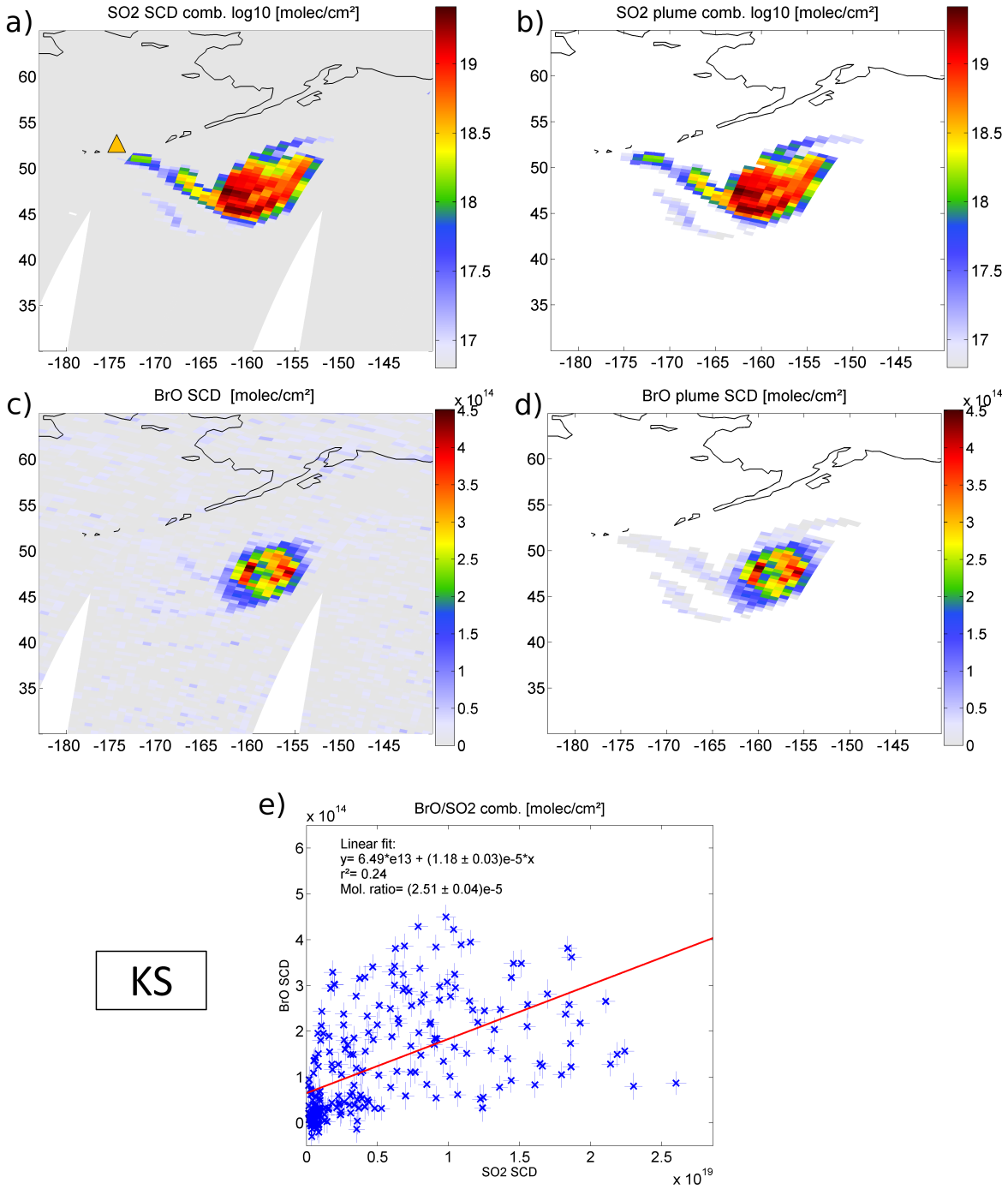

Fig. 11. SO_2 and BrO SCDs during the second day of the Kasatochi eruption (9 August 2008). While the SO_2 plume (**a** and **b**) and the enhanced BrO (**c** and **d**) are in principle located at the same area, the spatial distribution for BrO appears more circular than for the SO_2. The correlation plot **(e)** shows a positive correlation between the species ($r^2 = 0.24$), but also a large scatter in the BrO SCDs* with increasing SO_2 SCDs*.

measurements around 00:00 UTC on June 16. The resulting trajectory endpoints for the time of the GOME-2 observation can be seen in Fig. 14b and agree very well with the overall extent of the detected volcanic plume. Apparently, the plume's transport in opposite directions from the volcano results from different injection heights and a change in the wind direction from westerly to easterly between 11–13 km height. In Fig. 14c and d, the trajectory endpoints are additionally shown in comparison with the SCDs* of the combined SO_2 product as well as for BrO. A closer look to the

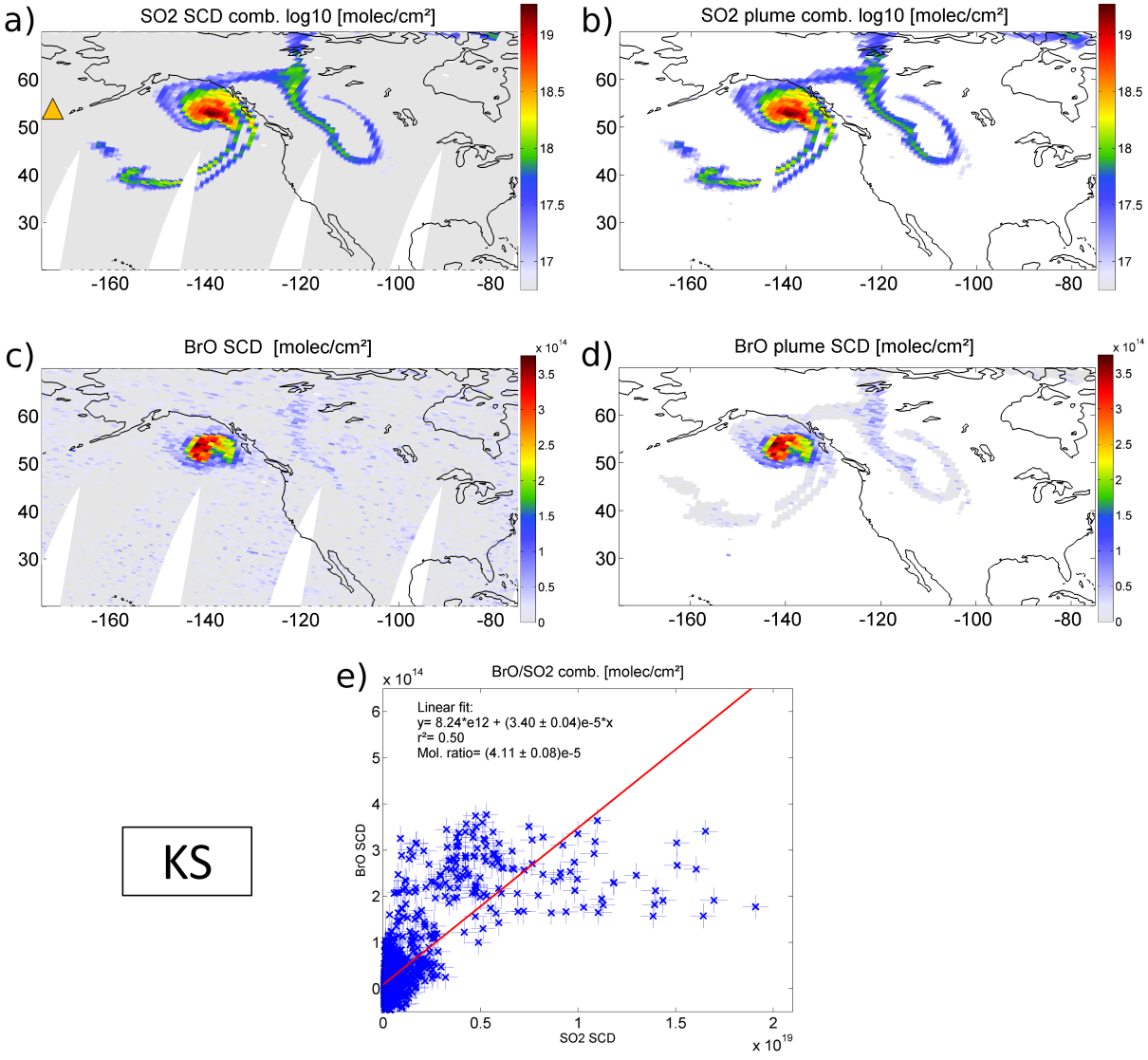

Fig. 12. GOME-2 maps for SO_2 and BrO for the volcanic plume of Kasatochi on 11 August 2008. The centre part of the plume has further travelled in eastern direction, several branches now extend from the plume centre in south western and north eastern direction (**a** and **b**). The enhanced BrO SCDs* are located around the centre region, but the distribution inside this area remains different compared to the one for SO_2 (**c** and **d**), as the highest SO_2 SCDs* appear directly in the plume centre, while the BrO seems to be twisted around it. This can also be seen in the correlation plot **(e)**, where the BrO columns are independently scattered around 2.5×10^{14} for SO_2 SCDs* $> 5 \times 10^{18}$ molec cm^{-2}.

trajectory endpoints reveals that the enhanced BrO SCDs* were most probably caused by the 3 explosions between 09:00–11:00 UTC on 15 June at plume heights of 6–8 km. One explanation for this behaviour could be that different volcanic mechanisms were involved during the individual explosions (compare to Sect. 4.4), leading to different injection heights and varying plume compositions. Furthermore, the bromine chemistry could be influenced by the meteorological parameters at different altitudes (e.g., temperature and relative humidity), which might have a crucial influence on the BrO formation process in addition to plume conditions like the presence of aerosol particles.

5 Systematic analysis of BrO events in volcanic plumes

In order to quantify the abundance of BrO in a more systematic way, we analysed the results from all captured volcanic plumes and divided them into different categories, each one representing a different class of BrO to SO_2 relationship (see Table 3).

In total, 64 individual volcanic plumes were found with indications for the presence of volcanic BrO of which all corresponding maps of the categorised events are available in the attached Supplement. By looking at the results, it again becomes clear that each volcanic eruption/degassing event

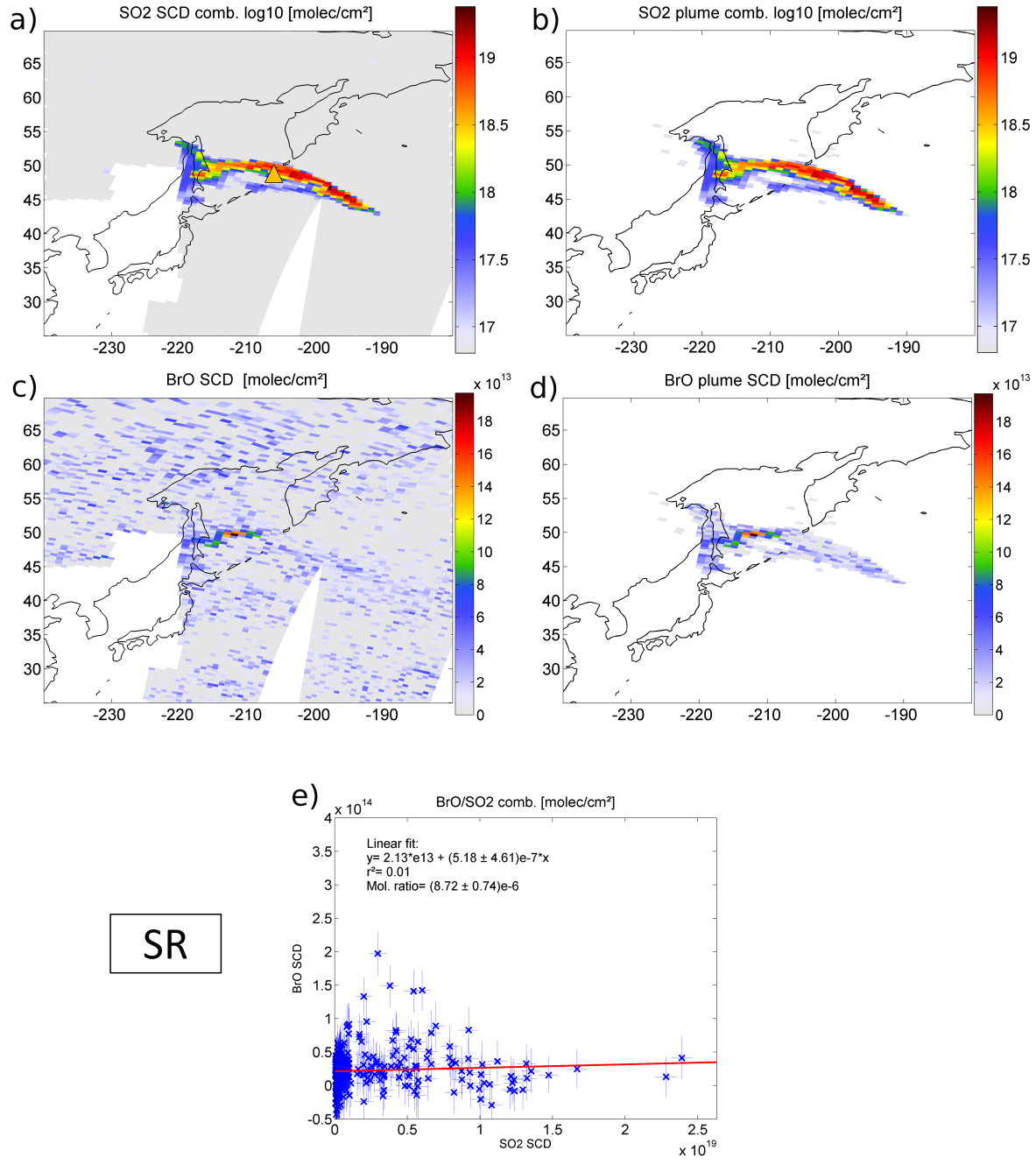

Fig. 13. The volcanic SO_2 and BrO plume during the eruption of Sarychev on 15/16 June 2009. The SO_2 plume (**a** and **b**) is transported in western and eastern direction from the volcano (indicated by the orange triangle in **(a)**; the white area in the lower left corner is due to data restrictions in order to prevent the detection of anthropogenic SO_2 over China). Surprisingly, enhanced BrO columns are only observed in a fraction of the western part (**c** and **d**). The correlation plot for both species, therefore, lead to an r^2 value close to zero from the bivariate linear fit (13e).

has its own specific circumstances (see also Sects. 4.1–4.6). For a more detailed analysis of the individual plumes, it will be necessary to perform several case studies in the future, taking into account the influence of volcanic ash, the age of the plume and the plume's height distribution with the corresponding meteorological parameters, such as the ambient air temperature and relative humidity. Here, we limit ourselves to a brief overview of the results.

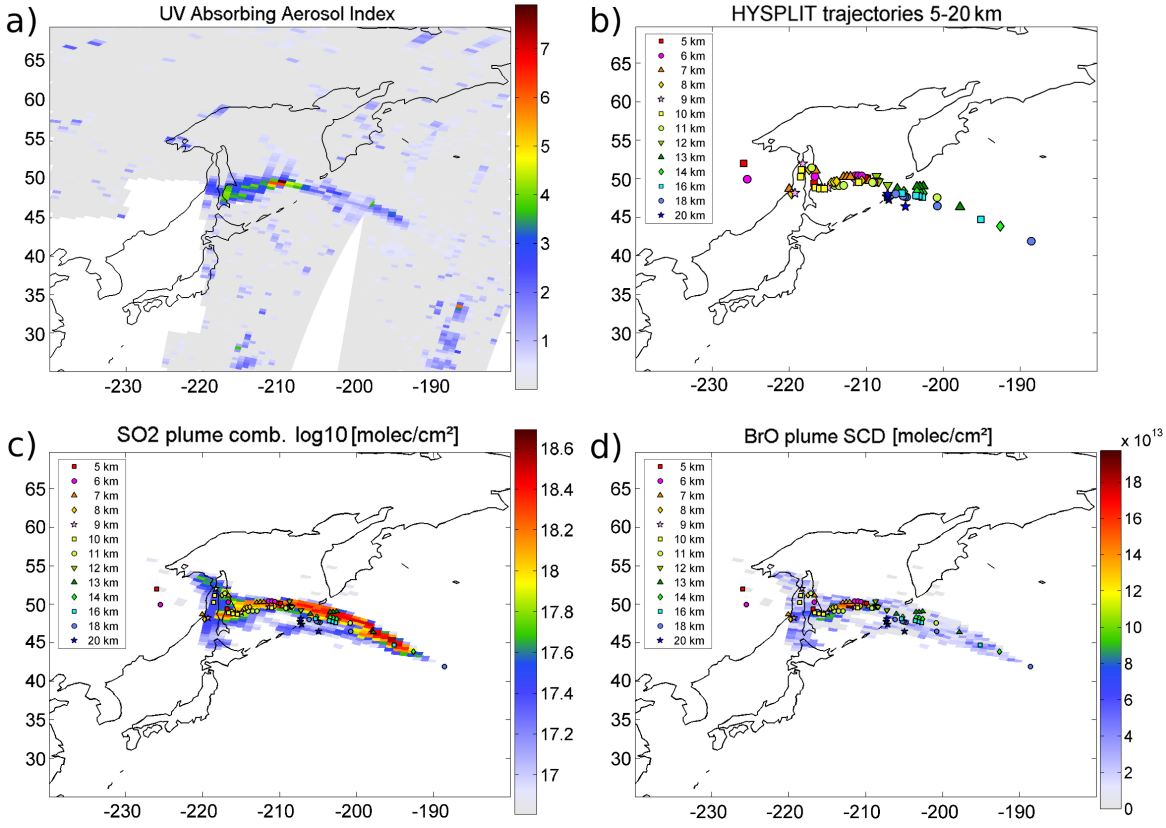

Fig. 14. (a) UV Absorbing Aerosol Index (AAI) for the Sarychev eruption on 15/16 June 2009. Like for BrO, the highest values occur in the western part of the plume, indicating an ash-rich explosion in temporal proximity to the satellite measurements. **(b)** HYSPLIT trajectory endpoints for starting heights between 5 and 20 km of the last 5 major explosions during the two days before the GOME-2 measurements took place. The trajectory simulations point out, that the wind changed from western to eastern direction between 11 and 13 km with increasing height. **(c)** Overlap of the volcanic SO_2 plume from the combined retrieval with the trajectory endpoints. **(d)** Overlap of the BrO_2 SCDs* in the area of the captured SO_2 plume with the trajectory endpoints.

Table 3. Categories that were used for the BrO/SO_2 analysis of all detected volcanic plumes.

category	description	r^2	p value	BrO VCD^*_{max}	BrO cluster	number of events
I	clear linear BrO/SO_2 correlation	>0.5	$<5 \times 10^{-3}$	$>2\sigma^*$	3-pixel cluster with VCD* $>2\sigma^*$	17
II	weak linear BrO/SO_2 correlation	≥ 0.25	$<1 \times 10^{-3}$	$>2\sigma^*$	3-pixel cluster with VCD* $>2\sigma^*$	23
III	nonlinear BrO/SO_2 relation	≤ 0.25	–	$>4\sigma^*$	6-pixel cluster with VCD* $>2\sigma^*$	24
IV	no enhanced BrO	–	–	–	–	708

5.1 Category I: clear linear correlation

All captured volcanic plumes that showed signs for a clear linear BrO to SO_2 correlation by a correlation coefficient $r^2 > 0.5$, a corresponding p value $< 5 \times 10^{-3}$ (Davidson and MacKinnon, 1993) and a maximum BrO VCD* $>2\sigma^*$ were collected in category I. Additionally, the results were restricted to plume events that contained a cluster of at least 3 neighbouring satellite pixels with BrO VCDs* $>2\sigma^*$. Table 4 lists the 17 volcanic events that were identified as part of category I, containing individual plumes from 6–8 different volcanoes. Apart from the eruptions that were already

Table 4. Category I (*clear linear correlation*) BrO/SO_2-analysis of all detected volcanic plumes of Category I. Columns contain: event number, volcano, measurement date, max. BrO SCD, max. SO_2 SCD, coincidence of max. SO_2 and BrO SCD, r^2, BrO/SO_2 slope, ratio of integrated BrO and SO_2 molecules, ratio of max. SO_2 and BrO SCD and coordinates of regarded area.

#	volcano	date	BrO SCD_{max} [molec cm^{-2}]	SO_2 SCD_{max} [molec cm^{-2}]	L^b	r^2	fitted BrO/SO_2	integrated BrO/SO_2	BrO_{max} $/SO_{2\,max}$	coordinates
22	Bezymianny[c]	11./12.05.2007	1.3×10^{14}	3.1×10^{17}	no	0.62	$(5.1 \pm 1.0) \times 10^{-4}$	$(3.7 \pm 0.5) \times 10^{-4}$	$(4.1 \pm 1.0) \times 10^{-4}$	[40–70° N, 145–180° E]
68[d]	Etna	24.11.2007	1.4×10^{14}	1.1×10^{18}	yes	0.61	$(1.1 \pm 0.3) \times 10^{-4}$	$(1.1 \pm 0.2) \times 10^{-4}$	$(1.3 \pm 0.3) \times 10^{-4}$	[20–49° N, 0–35° E]
94[a]	Etna	11.05.2008	2.3×10^{14}	1.5×10^{18}	yes	0.60	$(8.6 \pm 1.5) \times 10^{-5}$	$(1.2 \pm 0.2) \times 10^{-4}$	$(1.5 \pm 0.6) \times 10^{-4}$	[20–55° N, 5–45° E]
97	Etna	14.05.2008	2.4×10^{14}	8.2×10^{17}	yes	0.70	$(2.7 \pm 0.2) \times 10^{-4}$	$(2.1 \pm 0.1) \times 10^{-4}$	$(3.0 \pm 0.3) \times 10^{-4}$	[20–60° N, −5–35° E]
164[a]	Kasatochi	11.08.2008	3.7×10^{14}	1.9×10^{19}	no	0.50	$(3.4 \pm 0.0) \times 10^{-5}$	$(4.1 \pm 0.1) \times 10^{-5}$	$(2.0 \pm 0.1) \times 10^{-5}$	[20–70° N, 60–180° W]
282[a]	Redoubt	26.03.2009	1.9×10^{14}	5.8×10^{18}	yes	0.90	$(3.5 \pm 0.9) \times 10^{-5}$	$(4.7 \pm 1.1) \times 10^{-5}$	$(3.4 \pm 0.9) \times 10^{-5}$	[40–70° N, 135–170° W]
322	Redoubt	18.04.2009	1.1×10^{14}	4.8×10^{17}	no	0.62	$(2.3 \pm 0.4) \times 10^{-4}$	$(1.9 \pm 0.2) \times 10^{-4}$	$(2.5 \pm 0.7) \times 10^{-4}$	[35–70° N, 135–170° W]
363	Redoubt	29.05.2009	9.1×10^{13}	3.8×10^{17}	yes	0.56	$(2.5 \pm 0.9) \times 10^{-4}$	$(1.9 \pm 0.5) \times 10^{-4}$	$(2.4 \pm 0.9) \times 10^{-4}$	[45–70° N, 135–170° W]
535	Ambrym	08.04.2010	6.7×10^{13}	3.0×10^{17}	no	0.70	$(3.4 \pm 1.3) \times 10^{-4}$	$(1.1 \pm 0.7) \times 10^{-4}$	$(2.2 \pm 1.2) \times 10^{-4}$	[0–35° S, 150–185° E]
541	Eyjafjallajökull	23.04.2010	1.6×10^{14}	3.7×10^{17}	yes	0.65	$(5.9 \pm 1.8) \times 10^{-4}$	$(2.4 \pm 0.7) \times 10^{-4}$	$(4.4 \pm 1.3) \times 10^{-4}$	[45–70° N, 0–35° W]
545	Eyjafjallajökull	25.04.2010	1.3×10^{14}	4.6×10^{17}	no	0.75	$(3.4 \pm 0.9) \times 10^{-4}$	$(3.0 \pm 0.5) \times 10^{-4}$	$(3.0 \pm 0.9) \times 10^{-4}$	[45–70° N, 0–35° W]
546	Eyjafjallajökull	26.04.2010	8.8×10^{13}	4.2×10^{17}	yes	0.58	$(2.7 \pm 1.4) \times 10^{-4}$	$(1.9 \pm 0.8) \times 10^{-4}$	$(2.1 \pm 1.0) \times 10^{-4}$	[45–70° N, 0–35° W]
550	Eyjafjallajökull	29.04.2010	1.3×10^{14}	6.1×10^{17}	yes	0.54	$(1.9 \pm 0.5) \times 10^{-4}$	$(1.1 \pm 0.3) \times 10^{-4}$	$(2.1 \pm 0.7) \times 10^{-4}$	[40–70° N, 0–45° W]
563	Ambrym	11.05.2010	8.6×10^{13}	6.4×10^{17}	yes	0.59	$(1.6 \pm 0.6) \times 10^{-4}$	$(9.5 \pm 4.2) \times 10^{-5}$	$(1.3 \pm 0.6) \times 10^{-4}$	[0–35° S, 150–190° E]
675	Kliuchevskoi[c]	29./30.03.2011	1.3×10^{14}	6.0×10^{17}	yes	0.79	$(2.6 \pm 0.9) \times 10^{-4}$	$(1.5 \pm 0.4) \times 10^{-4}$	$(2.2 \pm 0.9) \times 10^{-4}$	[40–70° N, 145–180° E]
700	Kizimen[c]	08./09.05.2011	8.8×10^{13}	3.3×10^{17}	no	0.56	$(2.9 \pm 1.3) \times 10^{-4}$	$(1.9 \pm 0.7) \times 10^{-4}$	$(2.6 \pm 1.4) \times 10^{-4}$	[40–70° N, 140–180° E]
740	Kizimen[c]	07.06.2011	6.8×10^{13}	1.6×10^{17}	yes	0.63	$(5.0 \pm 4.5) \times 10^{-4}$	$(2.3 \pm 1.2) \times 10^{-4}$	$(4.1 \pm 2.8) \times 10^{-4}$	[40–70° N, 145–180° E]

[a] combined SO_2 product in case of high SO_2 SCDs $\geq 1 \times 10^{18}$ [molec cm^{-2}].
[b] location of SO_2 SCD_{max} is the same as for BrO SCD_{max}.
[c] corresponding volcano cannot be clearly identified.
[d] SO_2 SCDs $\geq 1 \times 10^{18}$ [molec cm^{-2}], but no plume pixels found in the SO_2 AR.

discussed in Sect. 4 (Bezymianny, Etna and Kasatochi), plumes from eruptions of Redoubt and Eyjafjallajökull were identified. Additionally, another plume from an eruption of Etna at the end of November 2007 and two further eruptions on Kamchatka were detected. Like for the already discussed case of the Bezymianny volcano (event No. 22 in Table 4 – see Sect. 4.2), we cannot be completely sure if the named volcanoes were really responsible for the detected volcanic plumes. In case of the Kliuchevskoi eruption on 29/30 March 2011 (event No. 675 in Table 4), the volcanic plume extended over an area of approximately 250 km in latitudinal direction of Kamchatka's eastern coast (encompassing the Kliuchevskoi, Kizimen and Shiveluch volcanoes). While Bezymianny showed no increased activity, the Kizimen volcano (about 100 km south) and the Shiveluch volcano (approximately 80 km north-east) had periods of significant unrest, as reported by KVERT. The location of the maximum SO_2 SCDs* and an additional report from the Volcanic Ash Advisory Center Tokyo (VAAC Tokyo) about a possible eruption from Kliuchevskoi on 30 March indicate, that the major part of the volcanic plume most probably came from Kliuchevskoi (Smithsonian, 2007–2011). For the volcanic plume events over Kamchatka on 8/9 May 2011 (event No. 700 in Table 4) and 7 June 2011 (event No. 740 in Table 4), none of the activity reports from the KVERT can give a clear preference regarding the responsible volcano, but the location of the main parts of the plumes as seen by the OMI instrument indicate that the corresponding eruptions occurred more likely at Kizimen than at the Shiveluch volcano, which also showed increased activity at the same time. For almost all of the category I cases, it is obvious that BrO of volcanic origin was present in the plume, as the BrO SCDs* were clearly enhanced in the area of enhanced SO_2. For most cases, the BrO columns even showed a quite similar spatial pattern compared to the SO_2 SCDs*, indicating a direct one-to-one correlation between the two species. However, it should be pointed out that the presence of enhanced BrO is not that clear for the volcanic plumes of the Ambrym volcano (event No. 535 and No. 563 in Table 4) in comparison to the other events in this category. Figure 15a shows the SO_2 plume from a strong degassing event of Ambrym on 8 April 2010. While the captured SO_2 plume consists only of a few satellite pixels (but can be clearly seen in the map), the BrO map shows no increased values at first sight, since all BrO SCDs* appear randomly scattered in the whole regarded area (Fig. 15c). This point-of-view changes by looking only at the area of captured SO_2 plume pixels (Fig. 15b and d). Although the BrO SCDs* in the plume's area are not well above the SCDs* in the reference area, a similar pattern can be seen in the distribution of the two species. The correlation plot (Fig. 15e) yields a surprisingly clear linear correlation, with $r^2 = 0.7$ and a relatively high mean BrO/SO_2 ratio of $(3.4 \pm 1.3) \times 10^{-4}$. While the r^2 in this example is one of the highest of all events in category I, it is worth noting that it is also the event with the lowest measured maximum BrO SCD*. The example, therefore, demonstrates that the algorithm seems to be capable to detect relatively low BrO columns produced by a strongly degassing volcano. Nevertheless, the associated error is rather large due to the BrO SCDs close to the detection limit.

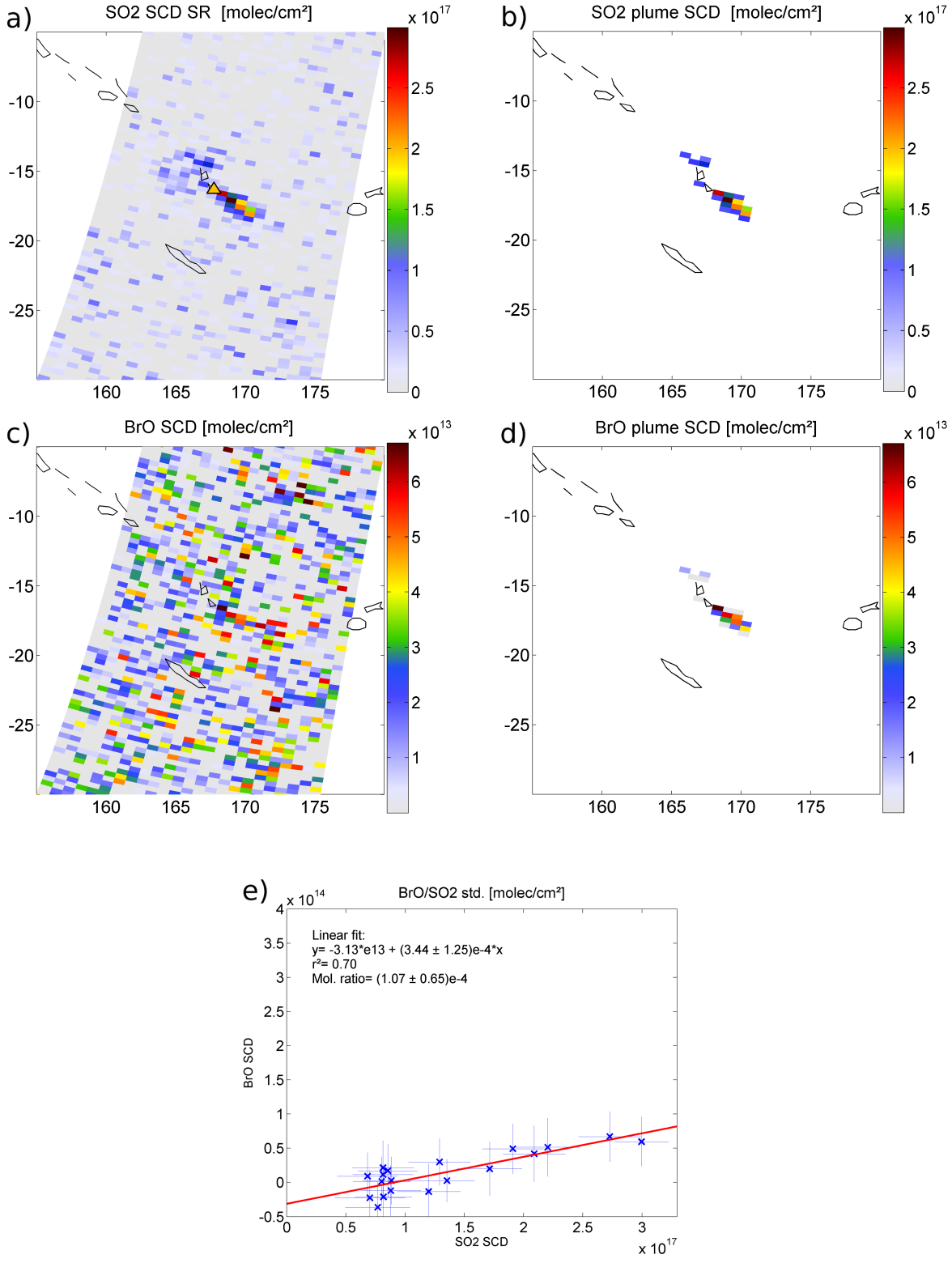

Fig. 15. SO_2 and BrO SCDs during a phase of enhanced passively degassing from the Ambrym volcano on 8 April 2010. While the SO_2 plume can be clearly seen in the satellite data **(a)**, enhanced BrO columns are not observed at first sight, since the large scatter indicates values around the instrument's detection limit **(c)**. By focusing on the area of extracted SO_2 plume pixels (**b** and **d**), the correlation plot for both species shows a surprisingly clear linear correlation with a resulting $r^2 = 0.7$ and a relatively high mean BrO/SO_2 ratio of $(3.44 \pm 1.25) \times 10^{-4}$ from the bivariate linear fit **(e)**.

Table 5. Category II (*weak linear correlation*) BrO/SO_2-analysis of all detected volcanic plumes of Category II. Columns contain: event number, volcano, measurement date, max. BrO SCD, max. SO_2 SCD, coincidence of max. SO_2 and BrO SCD, r^2, BrO/SO_2 slope, ratio of integrated BrO and SO_2 molecules, ratio of max. SO_2 and coordinates of regarded area.

#	volcano	date	BrO SCD_{max} [molec cm^{-2}]	SO_2 SCD_{max} [molec cm^{-2}]	L^b	r^2	fitted BrO/SO_2	integrated BrO/SO_2	BrO_{max} /SO_{2max}	coordinates
28	Kliuchevskoi	20./21.05.2007	5.1×10^{13}	1.9×10^{17}	no	0.40	$(2.9 \pm 1.3) \times 10^{-4}$	$(1.8 \pm 0.7) \times 10^{-4}$	$(2.6 \pm 1.4) \times 10^{-4}$	[40–70° N, 145–180° E]
48	Ambrym	16.07.2007	5.3×10^{13}	2.6×10^{17}	yes	0.38	$(2.4 \pm 1.0) \times 10^{-4}$	$(1.8 \pm 0.6) \times 10^{-4}$	$(2.1 \pm 1.0) \times 10^{-4}$	[0–35° S, 150–181° E]
163[a]	Kasatochi	10.08.2008	4.3×10^{14}	1.9×10^{19}	no	0.41	$(2.1 \pm 0.0) \times 10^{-5}$	$(3.1 \pm 0.1) \times 10^{-5}$	$(2.3 \pm 0.2) \times 10^{-5}$	[25–70° N, 110–185° W]
186	Kasatochi	20.08.2008	5.0×10^{13}	2.8×10^{17}	no	0.28	$(1.9 \pm 0.6) \times 10^{-4}$	$(1.5 \pm 0.3) \times 10^{-4}$	$(1.8 \pm 0.9) \times 10^{-4}$	[35–70° N, 160–180° W]
278[a]	Redoubt	23.03.2009	1.7×10^{14}	4.4×10^{18}	no	0.47	$(5.7 \pm 0.9) \times 10^{-5}$	$(7.8 \pm 0.6) \times 10^{-5}$	$(3.8 \pm 1.2) \times 10^{-5}$	[45–70° N, 115–170° W]
279	Redoubt	24.03.2009	1.1×10^{14}	1.0×10^{18}	no	0.50	$(1.1 \pm 0.1) \times 10^{-4}$	$(5.4 \pm 0.9) \times 10^{-5}$	$(1.1 \pm 0.3) \times 10^{-4}$	[45–70° N, 115–142° W]
281	Redoubt	26.03.2009	9.3×10^{13}	7.2×10^{17}	no	0.31	$(1.6 \pm 0.2) \times 10^{-4}$	$(1.4 \pm 0.1) \times 10^{-4}$	$(1.3 \pm 0.4) \times 10^{-4}$	[20–70° N, 85–130° W]
306	Redoubt	09.04.2009	8.5×10^{13}	3.3×10^{17}	no	0.41	$(3.8 \pm 0.9) \times 10^{-4}$	$(1.3 \pm 0.3) \times 10^{-4}$	$(2.5 \pm 1.0) \times 10^{-4}$	[40–70° N, 115–170° W]
312	Redoubt	13.04.2009	9.2×10^{13}	3.0×10^{17}	no	0.33	$(3.8 \pm 1.2) \times 10^{-4}$	$(2.4 \pm 0.4) \times 10^{-4}$	$(3.0 \pm 1.1) \times 10^{-4}$	[45–70° N, 135–170° W]
317	Redoubt	16.04.2009	1.4×10^{14}	5.1×10^{17}	yes	0.49	$(2.9 \pm 0.6) \times 10^{-4}$	$(2.3 \pm 0.3) \times 10^{-4}$	$(2.7 \pm 0.6) \times 10^{-4}$	[35–70° N, 140–180° W]
324	Redoubt	19.04.2009	6.7×10^{13}	3.3×10^{17}	no	0.33	$(2.8 \pm 0.9) \times 10^{-4}$	$(1.6 \pm 0.3) \times 10^{-4}$	$(2.0 \pm 0.9) \times 10^{-4}$	[50–70° N, 140–175° W]
344	Redoubt	05.05.2009	8.2×10^{13}	3.0×10^{17}	no	0.37	$(2.7 \pm 0.7) \times 10^{-4}$	$(1.6 \pm 0.3) \times 10^{-4}$	$(2.7 \pm 1.1) \times 10^{-4}$	[35–70° N, 140–175° W]
551	Eyjafjallajökull	30.04.2010	1.4×10^{14}	4.2×10^{17}	yes	0.50	$(3.2 \pm 0.8) \times 10^{-4}$	$(2.0 \pm 0.3) \times 10^{-4}$	$(3.3 \pm 1.0) \times 10^{-4}$	[40–70° N, −40–5° E]
555	Eyjafjallajökull	05.05.2010	1.7×10^{14}	7.2×10^{17}	no	0.34	$(1.2 \pm 0.2) \times 10^{-4}$	$(1.4 \pm 0.2) \times 10^{-4}$	$(2.5 \pm 0.6) \times 10^{-4}$	[35–70° N, −35–15° E]
557	Eyjafjallajökull	07.05.2010	1.0×10^{14}	5.5×10^{17}	no	0.29	$(1.6 \pm 0.3) \times 10^{-4}$	$(1.3 \pm 0.1) \times 10^{-4}$	$(1.9 \pm 0.7) \times 10^{-4}$	[20–70° N, −45–10° E]
558	Eyjafjallajökull	08.05.2010	9.5×10^{13}	5.7×10^{17}	no	0.26	$(1.6 \pm 0.3) \times 10^{-4}$	$(1.3 \pm 0.2) \times 10^{-4}$	$(1.7 \pm 0.8) \times 10^{-4}$	[25–70° N, 0–50° W]
568	Eyjafjallajökull	14.05.2010	1.3×10^{14}	8.4×10^{17}	no	0.42	$(1.4 \pm 0.2) \times 10^{-4}$	$(1.4 \pm 0.2) \times 10^{-4}$	$(1.6 \pm 0.6) \times 10^{-4}$	[35–70° N, −50–15° E]
570	Eyjafjallajökull	16.05.2010	1.2×10^{14}	3.5×10^{17}	no	0.32	$(3.9 \pm 0.9) \times 10^{-4}$	$(2.0 \pm 0.4) \times 10^{-4}$	$(3.5 \pm 1.3) \times 10^{-4}$	[35–70° N, −35–20° E]
572	Eyjafjallajökull	17.05.2010	1.5×10^{14}	7.3×10^{17}	no	0.42	$(2.9 \pm 0.4) \times 10^{-4}$	$(2.0 \pm 0.2) \times 10^{-4}$	$(2.1 \pm 0.6) \times 10^{-4}$	[35–70° N, −55–20° E]
696	Kizimen[c]	03.05.2011	6.6×10^{13}	3.7×10^{17}	yes	0.46	$(2.1 \pm 1.2) \times 10^{-4}$	$(1.2 \pm 0.6) \times 10^{-4}$	$(1.8 \pm 1.2) \times 10^{-4}$	[40–70° N, 140–175° E]
706	Kizimen[c]	21./22.05.2011	8.0×10^{13}	3.7×10^{17}	no	0.44	$(2.3 \pm 0.9) \times 10^{-4}$	$(2.1 \pm 0.5) \times 10^{-4}$	$(2.2 \pm 1.2) \times 10^{-4}$	[35–70° N, 140–175° E]
748	Nabro	15.06.2011	2.6×10^{14}	2.2×10^{19}	no	0.27	$(1.2 \pm 0.1) \times 10^{-5}$	$(1.7 \pm 0.2) \times 10^{-5}$	$(1.2 \pm 0.2) \times 10^{-5}$	[-10–65° N, 5–95° E]
749[a]	Nabro	16.06.2011	1.8×10^{14}	1.2×10^{19}	no	0.29	$(1.6 \pm 0.1) \times 10^{-5}$	$(1.9 \pm 0.3) \times 10^{-5}$	$(1.5 \pm 0.3) \times 10^{-5}$	[−15–60° N, 0–110° E]

[a] combined SO_2 product in case of high SO_2 SCDs $\geq 1 \times 10^{18}$ [molec cm^{-2}]
[b] location of SO_2 SCD_{max} is the same as for BrO SCD_{max}.
[c] corresponding volcano cannot be clearly identified.

5.2 Category II: weak linear correlation

In category II, all captured volcanic plumes that showed a weak linear BrO to SO_2 correlation were collected. The events in this category were characterised by a correlation coefficient $0.25 \geq r^2 < 0.5$, a corresponding p value $< 1 \times 10^{-3}$ (80 % lower than in category I) and a maximum BrO VCD* $> 2\sigma^*$ (see Table 5). Like for the first category, the results were restricted to plume events that showed a cluster of at least 3 neighbouring satellite pixels with BrO VCDs* $> 2\sigma^*$. For category II, in total 23 different volcanic events from 8-9 different volcanoes were identified. Some days during the eruptions of the highlighted volcanoes in Fig. 5 and 6 were detected (Kasatochi, Redoubt, Eyjafjallajökull and Nabro), but also plumes from eruptions on Kamchatka (Kliuchevskoi and Kizimen). However, the corresponding volcanoes for all plumes could easily be identified due to reports about specific explosion events shortly before the satellite measurements. In addition to several days during the eruptions of Redoubt and Eyjafjallajökull, also the third day after the eruption of Kasatochi was sorted into category II. Like in the examples in Sect. 4.5, the patterns of the enhanced BrO slant column densities look similar compared to those of SO_2, but a clear linear correlation between the two species is not found.

5.3 Category III: Nonlinear BrO/SO_2 relation

For the third category, the captured volcanic events were also investigated for plumes without signs of a linear correlation between SO_2 and BrO, but for which significantly enhanced BrO SCDs* were detected (correlation coefficient $r^2 \leq 0.25$). As no clear linear relationship is found for these cases, the threshold for the maximum BrO VCD* was increased to $4\sigma^*$, in order to assure an unambiguous detection of enhanced BrO in volcanic plumes. Additionally, the cluster size of neighbouring satellite pixels with BrO VCDs* $> 2\sigma^*$ (which is the criterion to identify a possible volcanic BrO plume) was raised from 3 to 6.

The identified plumes of category III can be seen in Table 6. In total 24 different volcanic events from 6 volcanoes were identified. For this category, only volcanic events were detected that had conspicuously high maximum BrO $VCDs^*_{max}$ in comparison to the SO_2 $VCDs^*_{max}$ in Fig. 5 (Kasatochi, Dalaffilla, Redoubt, Sarychev, Eyjafjallajökull and Nabro). As already pointed out for the examples in Sects. 4.3–4.6 (Figs. 9–13), most of these events only showed a roughly similar spatial pattern for both of the observed volcanic species. Especially for the eruptions of Kasatochi, Sarychev and Nabro, BrO could only be detected in some parts of the SO_2 plume for these volcanic events, resulting in low r^2 values from the linear fit. For such events, the BrO/SO_2 ratio calculated by the integrated number of molecules in the plume or the maximum SCDs is probably

Table 6. Category III (*eruptions with enhanced BrO cluster, but no linear correlation*) BrO/SO_2-analysis of all detected volcanic plumes of Category III. Columns contain: event number, volcano, measurement date, max. BrO SCD, max. SO_2 SCD, coincidence of max. SO_2 and BrO SCD, r^2, BrO/SO_2 slope, ratio of integrated BrO and SO_2 molecules, ratio of max. SO_2 and coordinates of regarded area.

#	volcano	date	BrO SCD_{max} [molec cm^{-2}]	SO_2 SCD_{max} [molec cm^{-2}]	L^b	r^2	fitted BrO/SO_2	integrated BrO/SO_2	BrO_{max} /SO_{2max}	coordinates
160[a]	Kasatochi	08.08.2008	3.6×10^{14}	3.9×10^{19}	no	0.22	$(4.4\pm0.3)\times10^{-6}$	$(1.2\pm0.0)\times10^{-5}$	$(9.3\pm0.7)\times10^{-6}$	[30–70° N, 145–195° W]
162[a]	Kasatochi	09.08.2008	4.5×10^{14}	2.6×10^{19}	no	0.24	$(1.2\pm0.0)\times10^{-5}$	$(2.5\pm0.0)\times10^{-5}$	$(1.7\pm0.1)\times10^{-5}$	[25–70° N, 135–190° W]
165[a]	Kasatochi	12.08.2008	3.0×10^{14}	1.6×10^{19}	no	0.21	$(2.4\pm0.1)\times10^{-5}$	$(3.2\pm0.1)\times10^{-5}$	$(1.9\pm0.2)\times10^{-5}$	[20–70° N, 50–175° W]
167[a]	Kasatochi	13.08.2008	1.3×10^{14}	1.5×10^{19}	no	0.14	$(9.7\pm0.4)\times10^{-6}$	$(2.5\pm0.1)\times10^{-5}$	$(9.0\pm1.9)\times10^{-6}$	[25–70° N, 20–175° W]
169[a]	Kasatochi	14.08.2008	1.1×10^{14}	6.9×10^{18}	no	0.00	$(-2.0\pm9.0)\times10^{-6}$	$(2.4\pm0.1)\times10^{-5}$	$(1.7\pm0.5)\times10^{-5}$	[20–70° N, −200–15° E]
249[a]	Dalaffilla	04.11.2008	1.7×10^{14}	4.3×10^{18}	no	0.01	$(1.1\pm0.3)\times10^{-5}$	$(4.0\pm0.3)\times10^{-5}$	$(3.9\pm0.8)\times10^{-5}$	[0–40° N, 30–70° E]
250[a]	Dalaffilla	05.11.2008	1.2×10^{14}	1.6×10^{18}	no	0.05	$(3.1\pm0.7)\times10^{-5}$	$(5.9\pm0.5)\times10^{-5}$	$(7.5\pm3.0)\times10^{-5}$	[−5–50° N, 25–100° E]
280	Redoubt	25.03.2009	1.2×10^{14}	1.0×10^{18}	no	0.25	$(8.8\pm1.3)\times10^{-5}$	$(1.1\pm0.1)\times10^{-4}$	$(1.2\pm0.4)\times10^{-4}$	[30–70° N, 100–140° W]
326	Redoubt	20.04.2009	9.1×10^{13}	4.2×10^{17}	no	0.17	$(3.1\pm0.7)\times10^{-4}$	$(2.5\pm0.3)\times10^{-4}$	$(2.2\pm0.9)\times10^{-4}$	[40–70° N, 135–170° W]
369[a]	Sarychev	12./13.06.2009	1.2×10^{14}	1.7×10^{18}	no	0.02	$(1.5\pm1.4)\times10^{-5}$	$(8.6\pm1.3)\times10^{-5}$	$(7.0\pm3.1)\times10^{-5}$	[30–65° N, 130–175° E]
370[a]	Sarychev	13./14.06.2009	1.0×10^{14}	3.9×10^{18}	no	0.01	$(-3.9\pm5.2)\times10^{-6}$	$(8.7\pm0.7)\times10^{-5}$	$(2.7\pm0.9)\times10^{-5}$	[25–70° N, 115–235° W]
375[a]	Sarychev	15./16.06.2009	1.9×10^{14}	2.3×10^{19}	no	0.01	$(1.5\pm1.4)\times10^{-5}$	$(8.7\pm0.7)\times10^{-6}$	$(8.3\pm1.4)\times10^{-6}$	[25–70° N, 120–180° E]
377[a]	Sarychev	16./17.06.2009	1.4×10^{14}	1.6×10^{19}	no	0.01	$(1.4\pm0.6)\times10^{-6}$	$(1.4\pm0.1)\times10^{-5}$	$(8.8\pm1.8)\times10^{-6}$	[20–70° N, 135–250° W]
378[a]	Sarychev	17./18.06.2009	1.6×10^{14}	1.1×10^{19}	no	0.01	$(2.0\pm0.7)\times10^{-6}$	$(2.2\pm0.2)\times10^{-5}$	$(1.4\pm0.3)\times10^{-5}$	[20–70° N, 115–250° W]
380[a]	Sarychev	19.06.2009	1.4×10^{14}	2.3×10^{18}	no	0.02	$(8.9\pm4.5)\times10^{-6}$	$(6.5\pm0.4)\times10^{-5}$	$(6.4\pm2.4)\times10^{-5}$	[45–70° N, 110–135° E]
548	Eyjafjallajökull	27.04.2010	1.1×10^{14}	3.1×10^{17}	no	0.07	$(1.1\pm1.5)\times10^{-5}$	$(3.6\pm0.5)\times10^{-4}$	$(3.6\pm1.3)\times10^{-4}$	[45–70° N, 0–40° W]
559	Eyjafjallajökull	09.05.2010	1.0×10^{14}	5.0×10^{17}	no	0.14	$(1.4\pm0.3)\times10^{-4}$	$(1.1\pm0.1)\times10^{-4}$	$(2.1\pm0.8)\times10^{-4}$	[25–70° N, −55–5° E]
560	Eyjafjallajökull	10.05.2010	9.8×10^{13}	3.8×10^{17}	no	0.12	$(1.3\pm0.3)\times10^{-4}$	$(1.0\pm0.1)\times10^{-4}$	$(2.6\pm1.2)\times10^{-4}$	[20–70° N, −50–5° E]
569	Eyjafjallajökull	15.05.2010	8.8×10^{13}	4.4×10^{17}	no	0.02	$(4.5\pm5.3)\times10^{-5}$	$(1.2\pm0.2)\times10^{-4}$	$(2.0\pm1.2)\times10^{-4}$	[40–70° N, 0–60° W]
745[a]	Nabro	13.06.2011	2.6×10^{14}	1.0×10^{19}	no	0.00	$(0.9\pm1.6)\times10^{-6}$	$(1.9\pm0.2)\times10^{-5}$	$(2.5\pm0.4)\times10^{-5}$	[−5–35° N, 10–60° E]
755[a]	Nabro	20.06.2011	1.4×10^{14}	5.6×10^{18}	no	0.12	$(3.0\pm0.4)\times10^{-5}$	$(2.4\pm0.4)\times10^{-5}$	$(2.6\pm0.9)\times10^{-5}$	[−20–55° N, −13–130° E]
758[a]	Nabro	21.06.2011	1.5×10^{14}	5.2×10^{18}	no	0.08	$(2.5\pm0.5)\times10^{-5}$	$(1.8\pm0.6)\times10^{-5}$	$(3.0\pm0.9)\times10^{-5}$	[−25–55° N, −15–90° E]
760[a]	Nabro	22.06.2011	1.1×10^{14}	3.8×10^{18}	yes	0.11	$(3.5\pm0.6)\times10^{-5}$	$(2.6\pm0.6)\times10^{-5}$	$(3.1\pm1.2)\times10^{-5}$	[−20–50° N, −20–100° E]
767[a]	Nabro	26.06.2011	1.2×10^{14}	3.6×10^{18}	yes	0.27	$(4.0\pm0.9)\times10^{-5}$	$(3.5\pm0.9)\times10^{-5}$	$(3.3\pm1.3)\times10^{-5}$	[−10–55° N, −4–75° E]

[a] combined SO_2 product in case of high SO_2 SCDs $\geq1\times10^{18}$ [molec cm^{-2}]
[b] location of SO_2 SCD_{max} is the same as for BrO SCD_{max}

better suited to give an estimate of the mean ratio (for events in category I and II, these alternative ratios are typically found to be similar as the ratio from the linear fit).

Besides the different plume ages and ambient conditions in the different parts of the plume, the distribution of enhanced BrO might also be caused by the significant ash content that was present during these eruptions and the associated heterogeneous chemical processes in the plume. For some of the detected events, the BrO SCDs* remain quite noisy, although the 6-neighbouring pixels criterion was fulfilled in parts of the plume. This is especially true for the second day after the Dalaffilla eruption (event No. 250 in Table 6), one day of the Redoubt eruption (event No. 326) and some days during the eruption of Eyjafjallajökull (event No. 559, No.560 and No. 569). In case of the Nabro eruption, the BrO SCDs* in the area of the captured SO_2 plume were well above the SCDs* in the corresponding reference area, but in contradiction to all other major eruptions, they could only be observed in the area close to the volcano for all detected days, where also the largest SO_2 SCDs* were detected (see Sect. 4.4). For the last 2 detected days of the Nabro eruption in June 2011, the location of the maximum SO_2 SCDs* from the combined SO_2 product (see also Sect. 3.5) matches the one for the maximum BrO SCDs*, which was not the case when using the SO_2 SR.

5.4 Category IV: volcanic plumes showing no enhanced BrO SCDs*

The majority of all captured plumes (92 %) showed no signs for the presence of volcanic BrO in the data, i.e., the retrieved BrO SCDs* were not enhanced with respect to the slant columns in the associated reference areas. This resulted in a correlation coefficient r^2 and a BrO/SO_2 ratio close to zero in such cases (the ratio was typically in the order of $<10^{-5}$ for such events). Figure 16 shows such an example for the eruption of the Fernandina volcano (Galapagos Island, Ecuador) on 13 April 2009. In Fig. 16a and c, the background corrected SCDs* for SO_2 and BrO are shown, including all pixels of the PEB cluster and the surrounding reference area. Accordingly, Fig. 16b and d show only the identified plume pixels for both species. The resulting correlation plot for the captured plume pixels (Fig. 16e) indicates no enhancement of BrO inside the plume.

6 Discussion and conclusions

Volcanic plumes were systematically extracted from the GOME-2 dataset during the time period between January 2007 and June 2011 (1642 days) by using SO_2 as a tracer for the plumes' extent. In total, 772 plumes on 553 days (34 % of all regarded days) could be detected in the data, caused by at least 37 different volcanoes. The subsequent analysis of the associated BrO SCDs within the SO_2 plumes

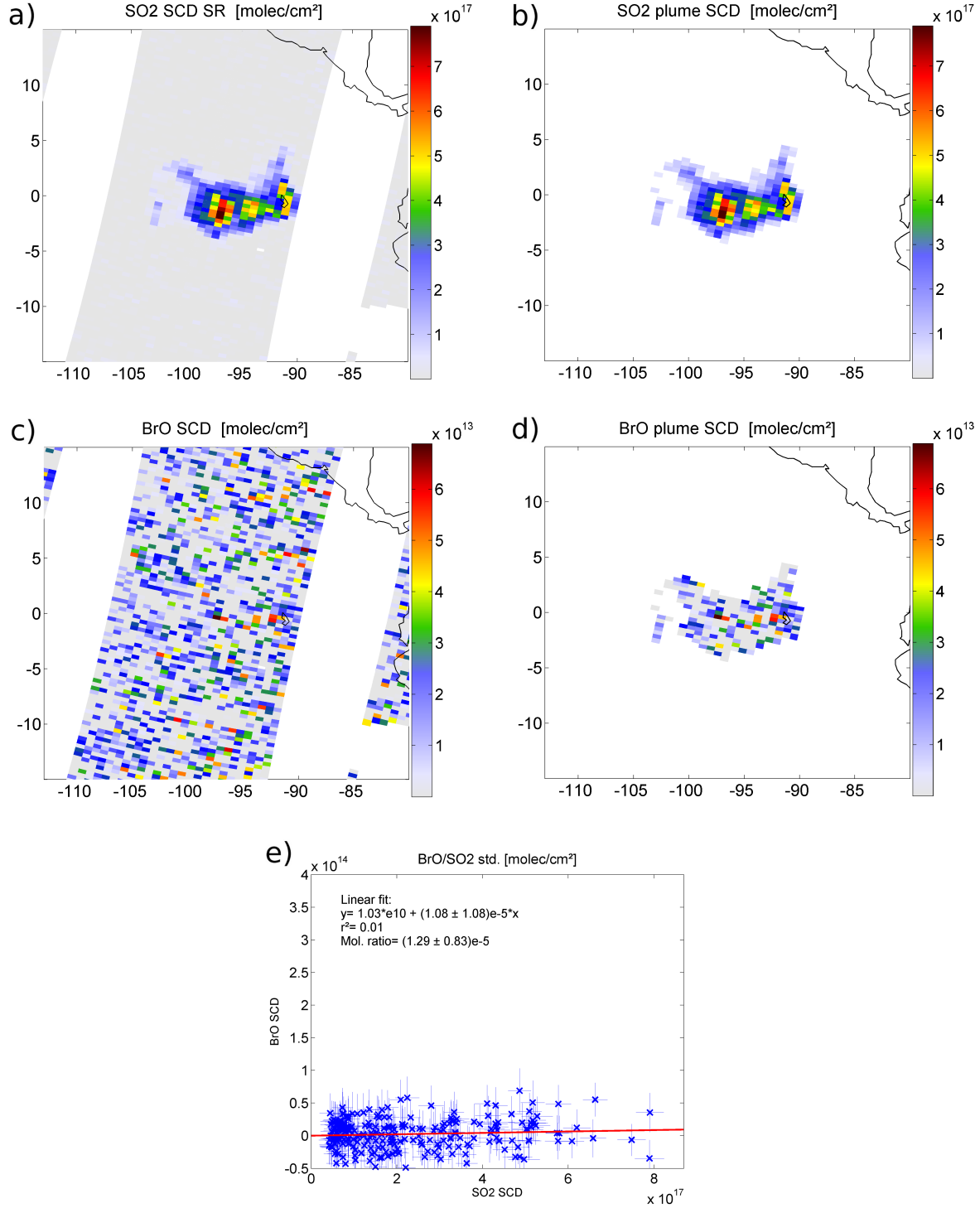

Fig. 16. SO_2 and BrO SCDs for the eruption of the Fernandina volcano (Galapagos Islands, Ecuador) on 13 April 2009. The background corrected SCDs* for SO_2 and BrO are shown (**a** and **c**), including the pixels of the PEB and the reference area. Accordingly, the extracted plume pixels are shown in **(b)** and **(d)**. The resulting correlation plot **(e)** shows no correlation between the two species as for the majority of all investigated plumes. The BrO SCDs* are statistically distributed over the whole area of the volcanic SO_2 plume, resulting in a vanishing correlation and a BrO/SO_2 ratio close to zero.

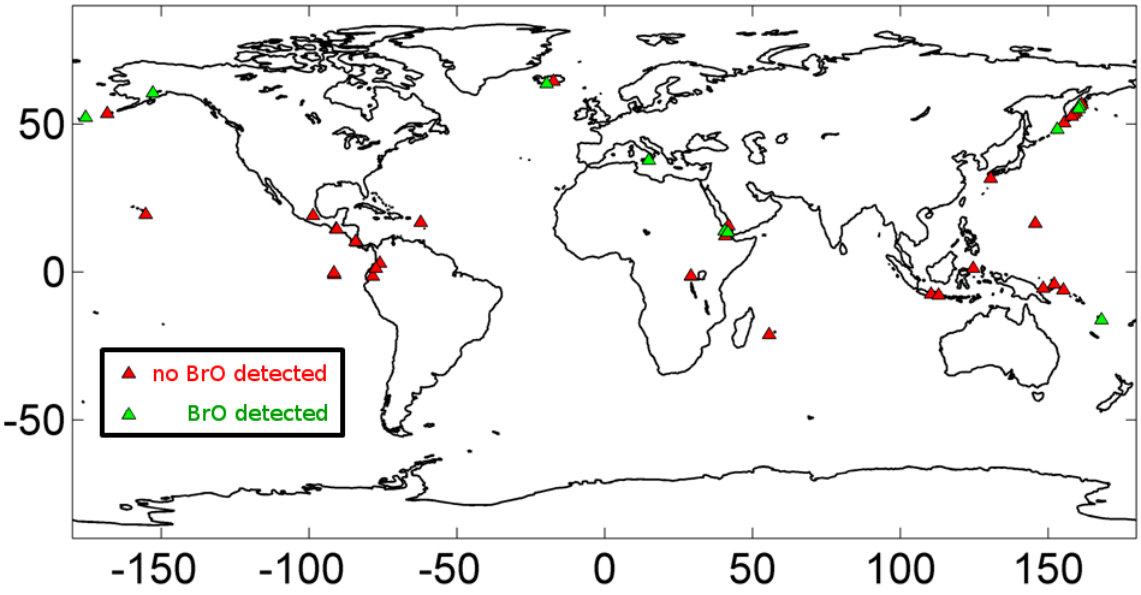

Fig. 17. Global map of the location of all volcanoes that were investigated within this study. In total, 64 volcanic plumes from 10–12 different volcanoes were found to show clear evidence for enhanced BrO column densities (green triangles). For all others, only SO_2 could be detected (red triangles).

demonstrates the capability of the GOME-2 instrument to monitor the abundance of volcanic BrO during moderate and major eruptions (or even very strong degassing events, whenever the BrO SCD is sufficiently high to exceed the instrument's detection limit). Overall, 64 volcanic plumes from 10-12 different volcanoes were found to show clear evidence for BrO of volcanic origin, which are about 8 % of all captured plumes and about 30 % of all volcanoes which emitted detectable SO_2 plumes. Figure 17 summarises the locations of all investigated volcanoes and highlights if enhanced BrO column densities were detected (green triangles) or only enhanced SO_2 could be observed (red triangles). For at least 5 volcanoes (Dalaffilla, Kizimen, Kliuchevskoi, Nabro and Sarychev) these are the first reported measurements of BrO to the authors' knowledge. Another detected BrO plume can most probably be assigned to the Bezymianny volcano on Kamchatka (event #22; see Sect. 4.2). Three more identified volcanic BrO plumes (events #675, #700 and #740) might have been caused by explosions at the Shiveluch volcano and another one (event #707) from Karymsky, although reports from KVERT in combination with OMI data suggest that Kliuchevskoi and Kizimen were most probably the origin of the detected plumes. This demonstrates clearly the advantage of satellite observations to monitor volcanic events in sparsely populated areas, where ground-based measurements are often difficult to realise (e.g., for Dalaffilla in Ethiopia or Nabro in Eritrea). For all other detected BrO plumes, the results confirm the general abundance of BrO at the corresponding volcanoes (Ambrym, Eyjafjallajökull, Kasatochi, Redoubt) as it has been found from former ground-based, airborne or satellite observations during recent years.

The total number of volcanoes where BrO has been detected by using UV-DOAS measurements can, therefore, be raised from 12 to 18 (for a survey of all former BrO observations see Kelly et al., 2012, and references therein).

It is important to point out that cases without significantly enhanced BrO SCDs can be caused by two different reasons:

1. The emissions of quiescent degassing volcanoes and/or during minor eruptions are too low. In such cases even if moderate or high BrO/SO_2 ratios are present in the plume, the BrO SCDs will be below the detection limit.

2. The BrO/SO_2 ratio is too low. This might be even the case for moderate or strong eruptions with high SO_2 SCDs. Regarding the top five of all 772 volcanic plumes with the largest SO_2 SCDs* in this study, two of them showed no evidence for the presence of volcanic BrO (Merapi on 5 November 2010 with a maximum SO_2 SCDs* of 8.9×10^{18}, respectively, Grímsvötn on 22 May 2011 with a maximum SO_2 SCDs* of 2.2×10^{19} molec cm^{-2}).

   However, from such cases, upper limits for the BrO/SO_2 ratio can be estimated by the ratio of the maximum BrO and SO_2 SCDs*, the ratio of total molecules or the resulting slope of the linear fit (the ratios can be found in the Supplementary Material for all investigated plumes). For the above mentioned cases of Merapi and Grímsvötn, the upper limits for the BrO/SO_2 ratios were found to be 8×10^{-6} and 2.5×10^{-6}, respectively.

Since satellite instruments usually have a relatively large footprint (40×80 km^2 for GOME-2), they are not able to

resolve small scale variations in the trace gas distribution. All measured columns of SO_2 and BrO need, therefore, to be interpreted as mean values within the area of a satellite pixel. This also implies that significantly higher BrO and SO_2 SCDs and probably also BrO/SO_2 ratios might have been present locally in the highlighted volcanic plumes.

6.1 Different BrO/SO_2 relationships

The collected examples of volcanic plumes show large variations of the BrO/SO_2 behaviour. For some of the identified plumes, the extent and shape of the BrO plume is roughly comparable to that of SO_2 and is accompanied by a similar distribution of the two species within the plume. This results in high values for the correlation coefficient ($r^2 > 0.5$) for the respective SCDs of the extracted plume pixels and allows us to determine the mean BrO/SO_2 ratio. Most of these cases were observed for moderate eruptions, where a well-defined compact plume was visible in the satellite data less than 24 h after the start of the associated eruption.

For other cases, only a weak linear correlation between BrO and SO_2 columns was observed that on the one hand may be caused by BrO SCDs that were only slightly above the instrument's detection limit, and on the other hand possibly due to the gradual chemical processing of aged volcanic plumes. For instance, in parts of the plume of the Dalaffilla eruption (Sect. 4.3), BrO was well correlated with SO_2, whereas in other parts no BrO was found. One explanation for this behaviour might be that not only the local composition of the volcanic plume (such as ash and/or other plume contents) have a crucial influence on the formation of BrO, but that the ambient meteorological conditions (temperature, relative humidity and plume height) also play an important role. This is also suggested by the results for the Sarychev eruption (see Sect. 4.6), where enhanced BrO SCDs were only observed in relative low plume heights of 6–8 km, but not at higher altitudes (>10 km), even if the largest SO_2 SCDs occurred here. It may also be that different volcanic mechanisms (e.g., energetic lava fountains, residual degassing) and the associated differences in the explosion intensity are responsible for higher/lower BrO enhancements at different altitudes.

The HYSPLIT trajectory analysis of the Sarychev case points out another problem that may show up especially during major eruptions. Passive DOAS instruments, such as GOME-2, SCIAMACHY and OMI often can not distinguish volcanic plumes at different altitude, but that overlap in the x-y-plane of observation. To investigate the influence of different ambient conditions on the formation of BrO in individual parts of the detected volcanic plumes, further trajectory calculations along with chemical model simulations will be necessary. Such simulations might be also used in order to analyse the temporal development of the BrO/SO_2 ratio and determine the lifetime for both species. This will be essential for the calculation of total SO_2 and BrO budgets in the future.

6.2 Comparison to previous ground-based/airborne measurements

Table 7 shows the BrO/SO_2 ratios for all former BrO observations by ground-based and airborne measurements side by side with those from this satellite study. The data are sorted by the corresponding volcanoes and the month of the measurements. Whenever the BrO/SO_2 ratio was determined more than once in a given month, the maximum ratio is shown. It should be emphasised that comparisons of satellite observations with ground-based measurements have to be interpreted with care, as they almost exclusively detect plumes from explosive eruptions, whereas ground-based observations usually investigate stable conditions at degassing volcanoes. Furthermore, the instruments exhibit very different viewing geometries and temporal resolutions. Ground-based observations of volcanic plumes are ideal for the investigation of the initial development of the BrO/SO_2 behaviour during the first minutes after the plume's release at quiescent degassing volcanoes, but the advantage of satellite instruments like GOME-2, SCIAMACHY and OMI lies in the ability to investigate this behaviour in entire volcanic plumes from moderate/major eruptions or strong degassing events on a much larger spatial and temporal scale. Nevertheless our results indicate that the BrO/SO_2 ratios during eruptions and periods of quiet degassing are not significantly different, as they were found to be similar to those from worldwide ground-based measurements with some 10^{-5} to several 10^{-4}. Satellite observations of the BrO/SO_2 ratios during volcanic eruptions may nevertheless lead to important additional conclusions regarding the applicability of BrO/SO_2 long-term measurements for the possible prediction of volcanic eruptions.

6.3 Comparison to previous satellite studies and future perspectives

An attempt to investigate the abundance of volcanic BrO using GOME and SCIAMACHY data by Afe et al. (2004) failed. As the spatial resolution of SCIAMACHY is better than for the GOME-2 instrument ($30 \times 60\,km^2$ compared to $40 \times 80\,km^2$), this result appears surprising. Meanwhile, the SCIAMACHY instrument has proven to be able to detect enhanced BrO SCDs of volcanic origin as well, as the BrO plume from Kasatochi was clearly visible in the data (Theys et al., 2009a).

In order to further investigate the potential of SCIAMACHY to detect BrO during volcanic events, we looked at BrO Level-2 data from the Belgian Institute for Space Aeronomy (Van Roozendael et al., 2006b) for all volcanic plumes with enhanced BrO SCDs that we had found in the GOME-2 data within this study (see Tables 4, 5 and 6). A considerable

Table 7. Table of worldwide reported volcanic BrO observations for different platforms, including the results from this study. The observations are sorted by the responsible volcano and the month of the corresponding measurements. For several measurements within a month, the maximum BrO/SO_2 ratios are always given (except Etna measurements by Bobrowski and Giuffrida (2012), showing mean ratios). Uncertain volcanoes are indicated by *.

date	volcano	BrO/SO_2 ratio	platform	reference
Jan 07	Ambrym	4.1×10^{-4}	airborne	Bani et al. (2009)
Mar 07		1.0×10^{-5}	airborne	Bani et al. (2009)
Jul 07		5.0×10^{-5}	airborne	Bani et al. (2009)
Jul 07		$(2.4 \pm 1.0) \times 10^{-4}$	satellite	this study
Aug 07		7.0×10^{-4}	airborne	Bani et al. (2009)
Apr 10		$(3.4 \pm 1.3) \times 10^{-4}$	satellite	this study
May 10		$(1.6 \pm 0.6) \times 10^{-4}$	satellite	this study
May 07	Bezymianny*	$(5.1 \pm 1.0) \times 10^{-4}$	satellite	this study
Nov 08	Dalaffilla	$(5.9 \pm 0.5) \times 10^{-5}$	satellite	this study
Dec 05	Erebus	2.5×10^{-4}	ground-based	Boichu et al. (2011)
Sep 03	Etna	4.8×10^{-4}	ground-based	Bobrowski and Platt (2007)
Aug 04		3.6×10^{-4}	ground-based	Bobrowski and Platt (2007)
Aug 04		1.9×10^{-4}	ground-based	Oppenheimer et al. (2006)
Sep/Oct 04		1.4×10^{-4}	ground-based	Bobrowski and Giuffrida (2012)
Apr 06		2.3×10^{-4}	ground-based	Bobrowski and Giuffrida (2012)
Jun 06		1.6×10^{-4}	ground-based	Bobrowski and Giuffrida (2012)
Jun 07		2.4×10^{-4}	ground-based	Bobrowski and Giuffrida (2012)
Aug 07		1.8×10^{-4}	ground-based	Bobrowski and Giuffrida (2012)
Sep 07		2.1×10^{-4}	ground-based	Bobrowski and Giuffrida (2012)
Oct 07		1.6×10^{-4}	ground-based	Bobrowski and Giuffrida (2012)
Nov 07		$(1.1 \pm 0.3) \times 10^{-4}$	satellite	this study
Feb 08		2.2×10^{-4}	ground-based	Bobrowski and Giuffrida (2012)
Apr 08		2.1×10^{-4}	ground-based	Bobrowski and Giuffrida (2012)
May 08		$(2.7 \pm 0.2) \times 10^{-4}$	satellite	this study
Apr 10	Eyjafjallajökull	$(5.9 \pm 1.8) \times 10^{-4}$	satellite	this study
May 10		1.3×10^{-4}	airborne, satellite	Heue et al. (2011)
May 10		2.1×10^{-4}	satellite	Rix et al. (2012)
May 10		$(3.9 \pm 0.9) \times 10^{-4}$	satellite	this study
Aug 08	Kasatochi	$(1.5 \pm 0.3) \times 10^{-4}$	satellite	this study
May 11	Kizimen*	$(2.9 \pm 1.3) \times 10^{-4}$	satellite	this study
May 07	Kliuchevskoi	$(2.9 \pm 1.3) \times 10^{-4}$	satellite	this study
Mar 11	Kliuchevskoi*	$(2.6 \pm 0.9) \times 10^{-4}$	satellite	this study
Mar 03	Masaya	8.0×10^{-5}	ground-based	Bobrowski and Platt (2007)
Apr 07		3.0×10^{-5}	ground-based	Kern et al. (2008)
Jun 11	Nabro	$(3.5 \pm 0.9) \times 10^{-5}$	satellite	this study
Mar 09	Redoubt	$(1.6 \pm 0.2) \times 10^{-4}$	satellite	this study
Apr 09		$(3.8 \pm 0.9) \times 10^{-4}$	satellite	this study
May 09		$(2.5 \pm 0.9) \times 10^{-4}$	satellite	this study
Aug 10		1.0×10^{-4}	airborne	Kelly et al. (2012)
May 04	Sakurajima	1.0×10^{-3}	ground-based	Lee et al. (2005)
Jun 09	Sarychev	$(8.6 \pm 1.3) \times 10^{-5}$	satellite	this study
Jun 11	Shiveluch*	$(2.3 \pm 1.2) \times 10^{-4}$	satellite	this study
May 02	Soufrière Hills	8.2×10^{-4}	ground-based	Bobrowski et al. (2003)
Sep 04	Stromboli	2.1×10^{-4}	ground-based	Bobrowski and Platt (2007)
Nov 04	Villarica	1.3×10^{-4}	ground-based	Bobrowski and Platt (2007)

fraction of the identified plume areas with enhanced BrO SCDs (36 %) was not covered by the SCIAMACHY instrument. Especially for the major eruptions of Sarychev and Nabro, the instrument missed the affected plume regions for almost all days, as the enhanced BrO columns occurred only in a relatively small area of about $10° \times 10°$, while the gaps in SCIAMACHY observations are typically $4° \times 15°$ in latitude and longitude, respectively. For all other volcanic plumes, the SCIAMACHY data indeed showed similar enhancements of the BrO SCDs in 90 % of these cases. Only for about 10 % of these events, the enhanced BrO columns were not clearly visible in the SCIAMACHY data, even though the instrument provided a sufficient coverage of the volcanic plume. However, in those cases the BrO SCDs were also close to the detection limit of the GOME-2 measurements.

The poor daily coverage of the instrument in combination with the comparatively short time period of about 18 months of SCIAMACHY data (33 scenes of volcanic SO_2 emissions from August 2002–January 2004) that were analysed in Afe et al. (2004) might be the main reason why their attempt failed. However, some of the proposed explanations for the lack of correlation between SO_2 and BrO columns in Afe et al. (2004) remain plausible and important, particularly because for the majority of GOME-2 measurements in the here presented study, no evidence for volcanic BrO was found either. The most important reasons are:

1. Current satellite instruments are usually not sensitive enough for the detection of BrO from steadily degassing volcanoes, especially not on daily basis. This is, for a large part, due to the coarse spatial resolution of these instruments, as a single ground pixel may cover an area that is much larger than the plume, causing the already small BrO SCDs to decrease. In most cases, only larger BrO plumes from moderate to major eruptions are detected. Furthermore, the sensitivity of satellite measurements decreases towards lower altitudes.

2. The formation rate and lifetime of BrO is influenced by several factors, like the plume height and the associated ambient meteorological conditions, the plume's composition and also probably the abundance of volcanic ash, which has an important influence on heterogeneous chemistry. While clearly enhanced BrO SCDs were, for example, detected after the Kasatochi eruption for several days thousands of kilometres from the volcano, this was only possible for a few hundred kilometres and approximately a plume age of 24h after the eruption of the Nabro volcano.

3. The fraction of halogen compounds of volcanic emissions and, thus, the amount of reactive halogen compounds in volcanic plumes may vary for individual volcanoes, so that the reactive bromine content for some of the space monitored eruptions is insufficient to form detectable amounts of BrO. Furthermore, the geophysical processes inside a volcano, such as the different solubility of bromine and sulphur in the melt depending on the movements of magma, might also play an important role for the initial BrO/SO_2 ratio during an eruption, as it was recently suggested by Bobrowski and Giuffrida (2012). Examples for very low BrO/SO_2 ratios are the major eruptions of Okmok (July 2008), Merapi (October/November 2010) and Grímsvötn (May 2011), with estimated upper limits in the range of 10^{-6} to 10^{-5}).

In the future, a detailed analysis of higher spatially resolved OMI data (available since October 2004 up to now with full daily global coverage) and the re-analysis of the entire SCIAMACHY data for the last 10 yr will probably increase the total number of volcanic BrO observations. In addition, the GOME-2 series will be completed by two additional instruments during the next 5–10 yr and provide further data in order to improve the spatial coverage and temporal resolution of volcanic monitoring from space. Furthermore, the Sentinel satellite series of the European Space Agency (ESA) will provide instruments with much higher spatial and temporal resolution for atmospheric monitoring (Sentinel-5 and Sentinel-5 precursor) and even one high resolution instrument on a geostationary satellite (Sentinel-4).

Supplementary material related to this article is available online at: http://www.atmos-chem-phys.net/13/4749/2013/acp-13-4749-2013-supplement.pdf.

Acknowledgements. We thank an anonymous referee and Robin Campion for helpful comments on the manuscript. Furthermore, we gratefully acknowledge Kornelia Mies and Rüdiger Sörensen from MPIC Mainz for technical support on the GOME-2 data. This work has been financially supported by the International Max Planck Research School for Atmospheric Chemistry and Physics, Mainz (Germany).

The service charges for this open access publication have been covered by the Max Planck Society.

Edited by: M. Van Roozendael

References

Afe, O. T., Richter, A., Sierk, B., Wittrock, F., and Burrows, J. P.: BrO emission from volcanoes: A survey using GOME and SCIAMACHY measurements, Geophys. Res. Lett., 31, 4 pp., doi:10.1029/2004GL020994, 2004.

Bani, P., Oppenheimer, C., Tsanev, V., Carn, S., Cronin, S., Crimp, R., Calkins, J., Charley, D., Lardy, M., and Roberts, T.: Surge in sulphur and halogen degassing from Ambrym volcano, Vanuatu, B. Volcanol., 71, 1159–1168, doi:10.1007/s00445-009-0293-7, 2009.

Barrie, L. A., Bottenheim, J. W., Schnell, R. C., Crutzen, P. J., and Rasmussen, R. A.: Ozone destruction and photochemical reactions at polar sunrise in the lower Arctic atmosphere, Published online: 14 July 1988; 334, 138–141, doi:10.1038/334138a0, 1988.

Bobrowski, N. and Giuffrida, G.: Bromine monoxide/sulphur dioxide ratios in relation to volcanological observations at Mt. Etna 2006–2009, Solid Earth, 3, 433–445, doi:10.5194/se-3-433-2012, 2012.

Bobrowski, N. and Platt, U.: SO_2/BrO ratios studied in five volcanic plumes, J. Volcanol. Geoth. Res., 166, 147–160, doi:10.1016/j.jvolgeores.2007.07.003, 2007.

Bobrowski, N., Hönninger, G., Galle, B., and Platt, U.: Detection of bromine monoxide in a volcanic plume, Nature, 423, 273–276, doi:10.1038/nature01625, 2003.

Bobrowski, N., von Glasow, R., Aiuppa, A., Inguaggiato, S., Louban, I., Ibrahim, O. W., and Platt, U.: Reactive halogen chemistry in volcanic plumes, J. Geophys. Res., 112, 17 pp., doi:10.1029/2006JD007206, 2007.

Bobrowski, N., Kern, C., Platt, U., Hörmann, C., and Wagner, T.: Novel SO_2 spectral evaluation scheme using the 360–390 nm wavelength range, Atmos. Meas. Tech., 3, 879–891, doi:10.5194/amt-3-879-2010, 2010.

Bogumil, K., Orphal, J., Homann, T., Voigt, S., Spietz, P., Fleischmann, O., Vogel, A., Hartmann, M., Kromminga, H., Bovensmann, H., Frerick, J., and Burrows, J.: Measurements of molecular absorption spectra with the SCIAMACHY pre-flight model: instrument characterization and reference data for atmospheric remote-sensing in the 230-2380 nm region, J. Photochem. Photobiol. A, 157, 167–184, doi:10.1016/S1010-6030(03)00062-5, 2003.

Boichu, M., Oppenheimer, C., Roberts, T. J., Tsanev, V., and Kyle, P. R.: On bromine, nitrogen oxides and ozone depletion in the tropospheric plume of Erebus volcano (Antarctica), Atmos. Environ., 45, 3856–3866, doi:10.1016/j.atmosenv.2011.03.027, 2011.

Bonaccorso, A., Bonforte, A., Calvari, S., Negro, C. D., Grazia, G. D., Ganci, G., Neri, M., Vicari, A., and Boschi, E.: The initial phases of the 2008–2009 Mount Etna eruption: A multidisciplinary approach for hazard assessment, J. Geophys. Res., 116, B03203, doi:10.1029/2010JB007906, 2011.

Bovensmann, H., Burrows, J. P., Buchwitz, M., Frerick, J., Noël, S., Rozanov, V. V., Chance, K. V., and Goede, A. P. H.: SCIAMACHY: Mission Objectives and Measurement Modes, J. Atmos. Sci., 56, 127–150, doi:10.1175/1520-0469(1999)056<0127:SMOAMM>2.0.CO;2, 1999.

Brenninkmeijer, C. A. M., Crutzen, P., Boumard, F., Dauer, T., Dix, B., Ebinghaus, R., Filippi, D., Fischer, H., Franke, H., Frieß, U., Heintzenberg, J., Helleis, F., Hermann, M., Kock, H. H., Koeppel, C., Lelieveld, J., Leuenberger, M., Martinsson, B. G., Miemczyk, S., Moret, H. P., Nguyen, H. N., Nyfeler, P., Oram, D., O'Sullivan, D., Penkett, S., Platt, U., Pupek, M., Ramonet, M., Randa, B., Reichelt, M., Rhee, T. S., Rohwer, J., Rosenfeld, K., Scharffe, D., Schlager, H., Schumann, U., Slemr, F., Sprung, D., Stock, P., Thaler, R., Valentino, F., van Velthoven, P., Waibel, A., Wandel, A., Waschitschek, K., Wiedensohler, A., Xueref-Remy, I., Zahn, A., Zech, U., and Ziereis, H.: Civil Aircraft for the regular investigation of the atmosphere based on an instrumented container: The new CARIBIC system, Atmos. Chem. Phys., 7, 4953–4976, doi:10.5194/acp-7-4953-2007, 2007.

Burton, M., Allard, P., Murè, F., and Oppenheimer, C.: FTIR remote sensing of fractional magma degassing at Mount Etna, Sicily, Geological Society, London, Special Publications, 213, 281–293, doi:10.1144/GSL.SP.2003.213.01.17, 2003.

Callies, J., Corpaccioli, E., Eisinger, M., Hahne, A., and Lefebvre, A.: GOME-2 – MetOp's Second Generation Sensor for Operational ozone Monitoring, ESA Bulletin, 102, 2000.

Cantrell, C. A.: Technical Note: Review of methods for linear least-squares fitting of data and application to atmospheric chemistry problems, Atmos. Chem. Phys., 8, 5477–5487, doi:10.5194/acp-8-5477-2008, 2008.

Davidson, R. and MacKinnon, J. G.: Estimation and Inference in Econometrics, Oxford University Press, 78–79, 1993.

De Smedt, I., Van Roozendael, M., and Jacobs, T.: Technical Note: Optimization of DOAS setings for BrO fitting from SCIAMACHY nadir spectra – Comparison with GOME BrO retrievals, Belgian Institute for Space Aeronomy (IASB-BIRA), Bruessels, Belgium, 32 pp., 2004.

Dikty, S. and Richter, A.: GOME-2 on MetOp-A Support for Analysis of GOME-2 In-Orbit Degradation and Impacts on Level 2 Data Products, final report, October 2011, http://www.eumetsat.int/groups/ops/documents/document/pdf_gome2_degrade_final_rep.pdf (last access: 12 September 2012), 2011.

Draxler, R. R. and Rolph, G. D.: HYSPLIT (HYbrid Single-Particle Lagrangian Integrated Trajectory) model access via NOAA ARL READY Webside, http://ready.arl.noaa.gov/HYSPLIT.php (last access: 12 September 2012), 2012.

EUMETSAT: GOME-2 Product Guide, http://oiswww.eumetsat.org/WEBOPS/eps-pg/GOME-2/GOME2-PG-index.htm, (last access: 12 September 2012), 2005.

Fan, S. and Jacob, D. J.: Surface ozone depletion in Arctic spring sustained by bromine reactions on aerosols, Nature, 359, 522–524, doi:10.1038/359522a0, 1992.

Galle, B., Bobrowski, N., Carn, S., Johansson, M., Kasereka, M., Oppenheimer, C., Yalire, M., and Zhang, Y.: Gas Emissions from Nyiragongo Volcano D.R. of Congo, measured by UV Mini-DOAS Spectroscopy, EGU meeting, http://www.cosis.net/abstracts/EGU05/08332/EGU05-J-08332.pdf (last access: 12 September 2012), 2005.

Gerlach, T. M.: Volcanic sources of tropospheric ozone-depleting trace gases, Geochem. Geophy Geosy, 5, 16 pp., doi:10.1029/2004GC000747, 2004.

Graaf, M. d., Stammes, P., Torres, O., and Koelemeijer, R. B. A.: Absorbing Aerosol Index: Sensitivity analysis, application to GOME and comparison with TOMS, J. Geophys. Res., 110, 19 pp., doi:10.1029/2004JD005178, 2005.

Graf, H., Feichter, J., and Langmann, B.: Volcanic sulfur emissions: Estimates of source strength and its contribution to the global sulfate distribution, J. Geophys. Res., 102, 10727–10738, doi:10.1029/96JD03265, 1997.

Greenblatt, G. D., Orlando, J. J., Burkholder, J. B., and Ravishankara, A. R.: Absorption Measurements of Oxygen Between 330 and 1140 nm, J. Geophys. Res., 95, 18577–18582, doi:10.1029/JD095iD11p18577, 1997.

Gür, B., Spietz, P., Orphal, J., and Burrows, J. P.: Absorption Spectra Measurements with the GOME-2 FMs using the IUP/IFE-UBs Calibration Apparatus for Trace Gas Absorption Spectroscopy VATGAS, Final Report, University of Bremen, October 2005,

2005.

Herman, J. R., Bhartia, P. K., Torres, O., Hsu, C., Seftor, C., and Celarier, E.: Global distribution of UV-absorbing aerosols from Nimbus 7/TOMS data, J. Geophys. Res., 102, 16911–16922, doi:10.1029/96JD03680, 1997.

Heue, K., Brenninkmeijer, C. A. M., Baker, A. K., Rauthe-Schöch, A., Walter, D., Wagner, T., Hörmann, C., Sihler, H., Dix, B., Frieß, U., Platt, U., Martinsson, B. G., van Velthoven, P. F. J., Zahn, A., and Ebinghaus, R.: SO_2 and BrO observation in the plume of the Eyjafjallajökull volcano 2010: CARIBIC and GOME-2 retrievals, Atmos. Chem. Phys., 11, 2973–2989, doi:10.5194/acp-11-2973-2011, 2011.

Houghton, B., McNutt, S., Rymer, H., and Stix, J.: Encyclopedia of Volcanoes, Academic Press Inc., edited by: Sigurdsson, H., 1417 pp., 2000.

Kelly, P. J., Kern, C., Roberts, T. J., Lopez, T., Werner, C., and Aiuppa, A.: Rapid chemical evolution of tropospheric volcanic emissions from Redoubt Volcano, Alaska, based on observations of ozone and halogen-containing gases, J. Volcanol. Geoth. Res., doi:10.1016/j.jvolgeores.2012.04.023, 2012.

Kern, C., Vogel, L., Rivera, C., Herrera, M., Platt, U., and Sihler, H.: Halogen oxide measurements at Masaya Volcano, Nicaragua using active long path differential optical absorption spectroscopy, B. Volcanol., 71, 659–670, doi:10.1007/s00445-008-0252-8, 2008.

Lee, C., Kim, Y. J., Tanimoto, H., Bobrowski, N., Platt, U., Mori, T., Yamamoto, K., and Hong, C. S.: High ClO and ozone depletion observed in the plume of Sakurajima volcano, Japan, Geophys. Res. Lett., 32, 4 pp., doi:10.1029/2005GL023785, 2005.

Levin, B. W., Rybin, A. V., Vasilenko, N. F., Prytkov, A. S., Chibisova, M. V., Kogan, M. G., Steblov, G. M., and Frolov, D. I.: Monitoring of the eruption of the Sarychev Peak Volcano in Matua Island in 2009 (central Kurile islands), Dokl. Earth Sci., 435, 1507–1510, doi:10.1134/S1028334X10110218, 2010.

Louban, I., Bobrowski, N., Rouwet, D., Inguaggiato, S., and Platt, U.: Imaging DOAS for volcanological applications, B. Volcanol., 71, 753–765, doi:10.1007/s00445-008-0262-6, 2009.

McConnell, J. C., Henderson, G. S., Barrie, L., Bottenheim, J., Niki, H., Langford, C. H., and Templeton, E. M. J.: Photochemical bromine production implicated in Arctic boundary-layer ozone depletion, Nature, 355, 150–152, doi:10.1038/355150a0, 1992.

Munro, R., Eisinger, M., Anderson, C., Callies, J., Carpaccioli, E., Lang, R., Lefevre, A., Livschitz, Y., and Albinana, A. P.: GOME-2 on MetOp, The 2006 EUMETSAT Meteorological Satellite Conference, Helsinki, Finland, 2006.

Neal, C. A., McGimsey, R. G., Dixon, J. P., Cameron, C. E., Nuzhaev, A. A., and Chibisova, M.: 2008 Volcanic activity in Alaska, Kamchatka, and the Kurile Islands: Summary of events and response of the Alaska Volcano Observatory: U.S. Geological Survey Scientific Investigations Report 2010-5243, http://pubs.usgs.gov/sir/2010/5243 (last access: 12 September 2012), 2011.

Ohno, M., Utsugi, M., Mori, T., Kita, I., Kagiyama, T., and Tanaka, Y.: Temporal variation in the chemical composition (HCl/SO_2) of volcanic gas associated with the volcanic activity of Aso Volcano, Japan, Earth Planet. Space, 65, e1–e4, doi:10.5047/eps.2012.11.003, 2013.

Oppenheimer, C., Tsanev, V., Braban, C., Cox, R., Adams, J., Aiuppa, A., Bobrowski, N., Delmelle, P., Barclay, J., and McGonigle, A.: BrO formation in volcanic plumes, Geochim. Cosmochim. Ac., 70, 2935–2941, doi:10.1016/j.gca.2006.04.001, 2006.

Penning de Vries, M. J. M., Beirle, S., and Wagner, T.: UV Aerosol Indices from SCIAMACHY: introducing the SCattering Index (SCI), Atmos. Chem. Phys., 9, 9555–9567, doi:10.5194/acp-9-9555-2009, 2009.

Platt, U. and Lehrer, E.: Arctic Tropospheric Ozone Chemistry, ARCTOC, Final Report of the EU-Project No. EV5V-CT93-0318, Heidelberg, 1996.

Platt, U. and Stutz, J.: Differential Optical Absorption Spectroscopy: Principles And Applications, Springer, 597 pp., 2008.

Pukīte, J., Kühl, S., Deutschmann, T., Platt, U., and Wagner, T.: Extending differential optical absorption spectroscopy for limb measurements in the UV, Atmos. Meas. Tech., 3, 631-653, doi:10.5194/amt-3-631-2010, 2010.

Richter, A.: Algorithm Theoretical Basis Document for the GOME-2 Rapid Volcanic SO_2 product, first draft, October 2009, http://www.doas-bremen.de/so2_alerts/gome2_so2_atbd_091005.pdf, (last access: 12 September 2012), 2009.

Richter, A., Wittrock, F., Ladstätter-Weissenmayer, A., and Burrows, J. P.: GOME measurements of stratospheric and tropospheric BrO, Adv. Space Res., 29, 1667–1672, doi:10.1016/S0273-1177(02)00123-0, 2002.

Richter, A., Wittrock, F., Schönhardt, A., and Burrows, J.: Quantifying volcanic SO_2 emissions using GOME-2 measurements, Poster at the EGU General Assembly 2009, 7679, XY247, http://www.iup.uni-bremen.de/doas/posters/egu_2009_richter.pdf, last access: 12 September 2012, 2009.

Rix, M., Valks, P., Hao, N., Loyola, D., Schlager, H., Huntrieser, H., Flemming, J., Koehler, U., Schumann, U., and Inness, A.: Volcanic SO_2, BrO and plume height estimations using GOME-2 satellite measurements during the eruption of Eyjafjallajökull in May 2010, J. Geophys. Res., 117, 19 pp., doi:10.1029/2011JD016718, 2012.

Rolph, G. D.: Real-time Environmental Applications and Display sYstem (READY) Website, http://ready.arl.noaa.gov (last access: 12 September 2012), 2012.

Rowland, F. S.: Stratospheric ozone depletion, Philosophical Transactions of the Royal Society B: Biological Sciences, 361, 769–790, doi:10.1098/rstb.2005.1783, 2006.

SACS: Support to Aviation Control Service, http://sacs.aeronomie.be (last access: 12 September 2012), 2012.

Schmincke, H.-U.: Volcanism, 1st ed. 2004. Corr. 2nd printing, 324 pp., ISBN 978-3-540-43650-8, Springer, 2005.

Sihler, H., Platt, U., Beirle, S., Marbach, T., Kühl, S., Dörner, S., Verschaeve, J., Frieß, U., Pöhler, D., Vogel, L., Sander, R., and Wagner, T.: Tropospheric BrO column densities in the Arctic derived from satellite: retrieval and comparison to ground-based measurements, Atmos. Meas. Tech., 5, 2779–2807, doi:10.5194/amt-5-2779-2012, 2012.

Simpson, W. R., von Glasow, R., Riedel, K., Anderson, P., Ariya, P., Bottenheim, J., Burrows, J., Carpenter, L. J., Frieß, U., Goodsite, M. E., Heard, D., Hutterli, M., Jacobi, H.-W., Kaleschke, L., Neff, B., Plane, J., Platt, U., Richter, A., Roscoe, H., Sander, R., Shepson, P., Sodeau, J., Steffen, A., Wagner, T., and Wolff, E.: Halogens and their role in polar boundary-layer ozone depletion, Atmos. Chem. Phys., 7, 4375-4418, doi:10.5194/acp-7-4375-2007, 2007.

Smithsonian: Global Volcanism Program, Smithsonian/USGS Weekly Volcanic Activity Reports 2007-2011, http://volcano.si.edu/reports/usgs/ (last access: 12 September 2012), 2007–2011.

Solomon, S.: Stratospheric ozone depletion: A review of concepts and history, Rev. Geophysics, 37, 275–316, doi:10.1029/1999RG900008, 1999.

Textor, C., Graf, H., and Timmreck, C.: Emissions from volcanoes, Kluwer Academic Publ., Dordrecht, the Netherlands, edited by: Granier, C., Artaxo, P., and Reeves, C. E., 18, 269–303, 2004.

Theys, N., Roozendael, M. V., Dils, B., Hendrick, F., Hao, N., and Maziŕe, M. D.: First satellite detection of volcanic bromine monoxide emission after the Kasatochi eruption, Geophys. Res. Lett., 36, 4 pp., doi:10.1029/2008GL036552, 2009a.

Theys, N., Roozendael, M. V., Errera, Q., Hendrick, F., Daerden, F., Chabrillat, S., Dorf, M., Pfeilsticker, K., Rozanov, A., Lotz, W., Burrows, J. P., Lambert, J.-C., Goutail, F., Roscoe, H. K., and Maziére, M. D.: A global stratospheric bromine monoxide climatology based on the BASCOE chemical transport model, Atmos. Chem. Phys., 9, 831–848, doi:10.5194/acp-9-831-2009, 2009b.

Theys, N., Van Roozendael, M., Hendrick, F., Yang, X., De Smedt, I., Richter, A., Begoin, M., Errera, Q., Johnston, P. V., Kreher, K., and De Mazière, M.: Global observations of tropospheric BrO columns using GOME-2 satellite data, Atmos. Chem. Phys., 11, 1791–1811, doi:10.5194/acp-11-1791-2011, 2011.

Theys, N., Campion, R., Clarisse, L., Brenot, H., van Gent, J., Dils, B., Corradini, S., Merucci, L., Coheur, P.-F., Roozendael, M. V., Hurtmans, D., Clerbaux, C., Tait, S., and Ferrucci, F.: Volcanic SO_2 fluxes derived from satellite data: a survey using OMI, GOME-2, IASI and MODIS, Atmos. Chem. Phys. Disc., 12, 31349–31412, doi:10.5194/acpd-12-31349-2012, 2012.

Torres, O., Bhartia, P. K., Herman, J. R., Ahmad, Z., and Gleason, J.: Derivation of aerosol properties from satellite measurements of backscattered ultraviolet radiation: Theoretical basis, J. Geophys. Res., 103, 17099–17110, doi:10.1029/98JD00900, 1998.

Van Roozendael, M., Loyola, D., Spurr, R., Balis, D., Lambert, J., Livschitz, Y., Valks, P., Ruppert, T., Kenter, P., Fayt, C., and Zehner, C.: Ten years of GOME/ERS-2 total ozone data—The new GOME data processor (GDP) version 4: 1. Algorithm description, J. Geophys. Res., 111, 21 pp., doi:10.1029/2005JD006375, 2006a.

Van Roozendael, M., Theys, N., and De Smedt, I.: SCIAMACHY BrO total column Product Specification Document, rev. 1, 30 January 2006, http://bro.aeronomie.be/Documents/BIRA_SCIA_BrO_PSD_v1r1.pdf, the data is freely available at http://bro.aeronomie.be/level2.php (last access: 12 September 2012), 2006b.

Vandaele, A. C., Hermans, C., Fally, S., Carleer, M., Colin, R., Mérienne, M., Jenouvrier, A., and Coquart, B.: High-resolution Fourier transform measurement of the NO_2 visible and near-infrared absorption cross sections: Temperature and pressure effects, J. Geophys. Res., 107, 12 pp., doi:10.1029/2001JD000971, 2002.

Vogel, L.: Volcanic plumes: Evaluation of spectroscopic measurements, early detection, and bromine chemistry, Ph.D. thesis, Combined Faculties for the Natural Sciences and for Mathematics, University of Heidelberg, 2012.

von Glasow, R.: Atmospheric chemistry in volcanic plumes, Proc. Natl.Acad. Sci., 107, 6594–6599, doi:10.1073/pnas.0913164107, 2010.

von Glasow, R. and Crutzen, P.: Tropospheric Halogen Chemistry, in: Treatise on Geochemistry, 1–67, Elsevier, 2003.

Wagner, T. and Platt, U.: Satellite mapping of enhanced BrO concentrations in the troposphere, Nature, 395, 486–490, doi:10.1038/26723, 1998.

Wagner, T., Beirle, S., and Deutschmann, T.: Three-dimensional simulation of the Ring effect in observations of scattered sun light using Monte Carlo radiative transfer models, Atmos. Meas. Tech., 2, 113–124, doi:10.5194/amt-2-113-2009, 2009.

Waythomas, C. F., Scott, W. E., Prejean, S. G., Schneider, D. J., Izbekov, P., and Nye, C. J.: The 7–8 August 2008 eruption of Kasatochi Volcano, central Aleutian Islands, Alaska, J. Geophys. Res., 115, doi:10.1029/2010JB007437, 2010.

Wennberg, P.: Atmospheric chemistry: Bromine explosion, Nature, 397, 299–301, doi:10.1038/16805, 1999.

Wilmouth, D. M., Hanisco, T. F., Donahue, N. M., and Anderson, J. G.: Fourier Transform Ultraviolet Spectroscopy of the A 2P3/2–X 2P3/2 Transition of BrO, J. Phys. Chem. A, 103, 8935–8945, doi:10.1021/jp991651o, 1999.

Yang, K., Krotkov, N. A., Krueger, A. J., Carn, S. A., Bhartia, P. K., and Levelt, P. F.: Retrieval of large volcanic SO_2 columns from the Aura Ozone Monitoring Instrument: Comparison and limitations, J. Geophys. Res., 112, 14 pp., doi:10.1029/2007JD008825, 2007.

Yang, K., Liu, X., Krotkov, N. A., Krueger, A. J., and Carn, S. A.: Estimating the altitude of volcanic sulfur dioxide plumes from space borne hyper-spectral UV measurements, Geophys. Res. Lett., 36, 6 pp., doi:10.1029/2009GL038025, 2009.